Daniel Alves Pinheiro

Development of a 3D printed prosthetic hand and forearm controlled by Arduino

Thesis to obtain the Master of Science Degree in Biomedical Engineering

Supervisors

Professor Doctor Rui Pedro Batoreo Amaral

Professor Doctor Ricardo Miguel Gomes Simões Baptista

December 2024

Daniel Alves Pinheiro

Development of a 3D printed prosthetic hand and forearm controlled by Arduino

Examination Commitee

***Chairperson**:*
Prof. Dr. Célio Gabriel Figueiredo Pina, Instituto Politécnico de Setúbal

***Supervisor**:*
Prof. Dr. Rui Pedro Batoreo Amaral, Instituto Politécnico de Setúbal,
Prof. Dr. Ricardo Miguel Gomes Simões Baptista, Instituto Superior Técnico

***Member of the Committee**:*
Prof. Dr. Manuel Mota Ferreira, Instituto Politécnico de Setúbal

December 2024

Acknowledgments

I'd like to start by thanking my two supervisors, Professor Rui Amaral and Professor Ricardo Baptista, for all their support, availability and patience. Without them, this work wouldn't have turned out the way it did, as they always helped me to overcome all the problems and difficulties. I will always be grateful for all the knowledge and advice they gave me and for giving me motivation to keep learning more and challenging my limits.

I would like to thank the EST Setúbal for the resources and tools provided, which were essential for carrying out this work.

To Professor Anna Letournel form providing the MYO armband and for her support. To Professor Carla Carneiro for providing the Peck Tech Multimeter and for her support. To all professors that help me in my academic career.

To my parents, brother and grandparents for their unconditional support throughout my academic career.

To my friends and laboratory colleagues Marta, Daniel, Carlos, Bruno, Adriana, Filipa, Ângela, Miguel, Rafael, Ruben and Gonçalo. For their support, company and help.

Resumo

A mão é uma ferramenta de elevada complexidade e a sua perda leva à total alteração de vida de um individuo. A perda desde membro faz com que a pessoa deixe de conseguir realizar as tarefas mais simples do quotidiano o que leva uma perda de qualidade de vida. A utilização de uma prótese é a solução proposta para este problema. Este trabalho tem como objetivo o desenvolvimento de uma mão protética fabricada por impressão 3D e controlada através de uma placa Arduíno. Tentando assim criar um produto acessível e efetivo.

O dispositivo foi desenhado utilizado o software Fusion 360 e impresso em PLA utilizando duas impressoras 3D, Prusa Mini Plus e Anycubic Kobra 2 Pro. A flexão e extensão dos cinco dedos é realizado por motores servo MG995 fixos no antebraço, que puxam fios presos na ponta de cada um. A abdução e adução do polegar é realizada por um motor servo SG90 embutido na mão. Os atuadores são controlados por joysticks, um para a rotação do antebraço e outro para flexão/extensão dos dedos e abdução/adução do polegar. Foram adicionados um sensor de temperatura e um de pressão, na ponta de cada dedo. Os sensores de pressão permitem que o sistema limite a força aplicada num objeto agarrado pela mão. Os sensores de temperatura permitem dar informação ao utilizador sobre a temperatura do objeto que está a segurar. Todos estes foram encapsulados na pontas dos dedos com silicone. O protótipo conseguiu realizar cinco gestos pré-programados e foi capaz de agarrar diversos objetos utlizados no quotidiano. Mostrou que o sistema de atuação necessita de ser otimizado, pois uso de cabos dificulta a realização de movimentos precisos. Grande parte da força aplicada pelos motores é utilizada para vencer a resistência destes cabos e o atrito entre componentes, reduzindo a eficiência do produto. A última etapa do trabalho está relacionada com o desenvolvimento de uma interface pessoa-máquina baseada no reconhecimento de gestos. Com base num conjunto de gestos pré-programados definidos, foi criado um corpus para treino e teste dos algoritmos. Os dados recolhidos foram segmentados e posteriormente foi feita a extração de características temperais e espectrais, nomeadamente RMS, VAR, STD e PSD. A classificação foi realizada por uma rede neuronal e *support vector machine* (SVM) tendo-se obtido uma precisão de 91,2% e 87,4% na classificação, respetivamente.

Conclui-se que mão prostética é capaz de realizar pelo menos cinco gesto pré-programado e de agarrar objetos do quotidiano. Apesar de se terem sido calibrados os sensores não se encontram ativos no protótipo e ainda é necessário a calibração dos sensores de pressão após a adição do silicone. Apesar dos resultados de AI esta componente ainda necessita de mais estudo para ser viável.

Palavras-chave: Impressão 3D; Arduíno; Próteses Mioelétricas; Machine Learning

Abstract

The hand is a highly complex tool, and its loss can completely change an individual's life. The loss of this limb means that the person is no longer able to perform the simplest everyday tasks, which leads to a loss of quality of life. The use of a prosthesis is the proposed solution to this problem. The aim of this work is to develop a prosthetic hand manufactured using 3D printing and controlled using an Arduino board. The aim is to create an affordable and effective product.

The device was designed using Fusion 360 software and printed in PLA using two 3D printers, Prusa Mini Plus and Anycubic Kobra 2 Pro. Flexion and extension of the five fingers is carried out by MG995 servo motors fixed to the forearm, which pull wires attached to the tip of each finger. Thumb abduction and adduction is performed by an SG90 servo motor built into the hand. The actuators are controlled by joysticks, one for forearm rotation and the other for finger flexion/extension and thumb abduction/adduction. A temperature sensor and a pressure sensor have been added to the tip of each finger. The pressure sensors allow the system to limit the force applied to an object gripped by the hand. The temperature sensors provide the user with information about the temperature of the object they are holding. All of these have been encapsulated in the fingertips with silicone. The last stage of the work is related to the development of a person-machine interface based on gesture recognition. Based on a set of pre-programmed gestures, a corpus was created for training and testing algorithms. The data collected was segmented and then temporal and spectral characteristics were extracted, namely RMS, VAR, STD and PSD. The classification tests were conducted using neural networks and support vector machines (SVM), with an accuracy of 91,2% and 87,4%, respectively.

It was concluded that the prosthetic hand can perform at least five pre-programmed gestures and hold everyday objects. Despite being tested, functional and mounted on the prototype, the sensor system is not active and the encapsulated pressure sensors still need to be calibrated. AI showed satisfactory results with a NN of 91,2% and an SVM of 84,7% but this component needs further study to be viable.

Keywords: 3D printing; Arduino; Myoelectric prostheses; Machine Learning

Table of Contents

Figures List

Tables List

Acronyms List

3D – Tridimensional

A.D – Anno Domi

ABS – Acrylonitrile Butadiene Styrene

ADC – Analog Digital Converter

AI – Artificial Intelligence

ANN – Artificial Neural Networks

BPPs – Body-Powered Prothesis

CAD – Computer Aided Design

CAM – Computer Aided Manufacture

DC – Direct Current

EST – Escola Superior de Technology (Superior School of Technology)

FFF – Fused Filament Fabrication

FNN – Feedforward Neural Network

FSR – Force Sensitive Sensors

G Code – Geometric Code

I2C – Inter-Integrated Circuit

IC – Integrated Circuit

IDE – Integrated Development Environment

Lda - Limitada (Limited)

LCD – Liquid Crystal Display

LEDs – Light-Emitting Diodes

MAV – Mean Absolute Values

Mhz – Mega Hertez

ML – Machine Learning

MUX – Multiplexer

nLSB – LM35 Sensor Bits Number

NN – Neural Networks

NTC – Negative Temperature Coefficient

NZC – Number Zero Crossing

OpAmps – Operational Amplifiers

PCB – Printed Circuit Board

PEEK – Polyether ether ketone

PLA – Polylactic Acid

PS – Power Spectrum

PSD - Power Spectral Density

PTC – Positive Temperature Coefficient

PWM – Pulse Width Modulation

Pro – Professional

RAM – Random Access Memory

Rf – Feedback Resistor

R – Resistance

R1 – Resistor 1

RMS – Root Mean Square

Rs – Source Resistor

SCL – Serial Clock Line

SDA – Serial Data Line

SDK – Software Development Kit

sEMG – Surface Electromyogram

SNR – Signal Noise Ratio

STD – Standard Deviation

SVM – Support Vector Machines

TPE – Thermoplastic Elastomer

USB – Universal Serial Bus

VAR – Variance

Vout – Output Voltage

ºC – Celsius Degrees

Chapter 1 - Introduction

This chapter makes an introduction to the main subject of the work by pointing it's motivation, what is the problem to be solved and what were the main objectives to achieve for the creation of a viable solution for this problem. It also contains a brief explanation on the thesis organization.

1.1. Motivation

The motivation behind this work development is the need for accessible and cost-effective prosthetic hands. While advanced robotic hands are often expensive and complex, the integration of 3D printing technology and Arduino microcontrollers offers an affordable and scalable alternative. Additionally, this work is also motivated by trying to create a device that will help who can't afford a state-of-the-art prosthetic.

1.2. Problem identification

The human hand allows for the performance of various daily tasks, having been an indispensable tool for the survival of human beings. Given the role of this anatomical member, its loss makes the lives of several people a constant suffering, for the simple fact of facing enormous difficulties in performing daily tasks, such as the putting on or taking off a piece of clothing. Normally the amputation of the hand is the product of some pathology such as infections, diabetes, cancer or trauma that the patient has suffered [1]. This leads the patients through a whole process of rehabilitation, their lives change completely due to the loss of the ability or need to relearn to perform tasks that they used to execute [2]. To help to minimize the challenges that amputees face prosthetics hands were created to simulate the function and appearance of the lost limb.

1.3. Objectives

The work main objective is to create a functional prosthetic hand using CAD and additive manufacturing, with the capability to grab objects having also the possibility of sensing heat and pressure applied to the grabbed object. To control this device, analogue joysticks will be use for the prototyping phase and for display purposes. A machine learning algorithm will be train using forearm myoelectric signal recognition to develop a human machine interface.

In order to design the prosthetic hand, several key steps are necessary: 1) first the design finger mechanisms, 2) second the manufacture of the finger and choosing the actuators, 3) third the addition of electronic components such as the sensors, the user interface and the control system, 4) fourth the acquisition and segmentation of myoelectric data for the two machine learning algorithms, support vector machine (SVM) and neural networks (NN), and 5) the final step will be the incorporation of the ML algorithms into the control system of the hand and the evaluation of each one shows the better accuracy.

1.4. Dissertation Organization

This thesis is divided into five main parts, the introduction, literature review, materials and methods, results and discussion, and conclusions. The introduction makes an approach of the work subject, explaining the motivation behind it, approaches the core objectives and explain how the work is organized. The literature review makes the reader aware of the different prosthetic hand on the market and other works in this field that utilize the same or a similar process during the work, approaches the methos and material used later in the work. The third chapter explains all the material used and methods that allow to achieve the final product. The results and discussion show and explain the results and how and why they were obtained comparing them to other work in the literature. The final chapter presented the reader the obtained conclusion in this work and the future perspectives for the project

Chapter 2 - Literature Review

This chapter makes an approach to robotic hands already in the market and to similar works, comparing the conventional methods to the additive manufacturing, pointing the benefits and the problems in each method to conclude which one performs better to the actual requirements and explains the manufacturing processes used to produce the prototype. Describes the main electronic components and their functions. On the final part of the chapter, an introduction to machine learning and to the classifier used in the project is made.

2.1. Prosthetic hands

Upper limb prothesis, are devices that try to mimic the function of a hand or arm, have their first record in 77 A.D on the encyclopaedia Naturalis Historia, written by the roman scholar Pliny the Elder. He describes that Marcus Sergius, a Roman general, who had lost his hand during the Second Punic War, had used an iron hand to substitute the lost limb, and that enabled him to return to the battle [3]. Another example of historic prosthetic hand is the iron hand of a German knight Götz von Berlichingen with articulated finger than could be posed by the user to hold weapon and horse reins (figure 1) [3], [4].

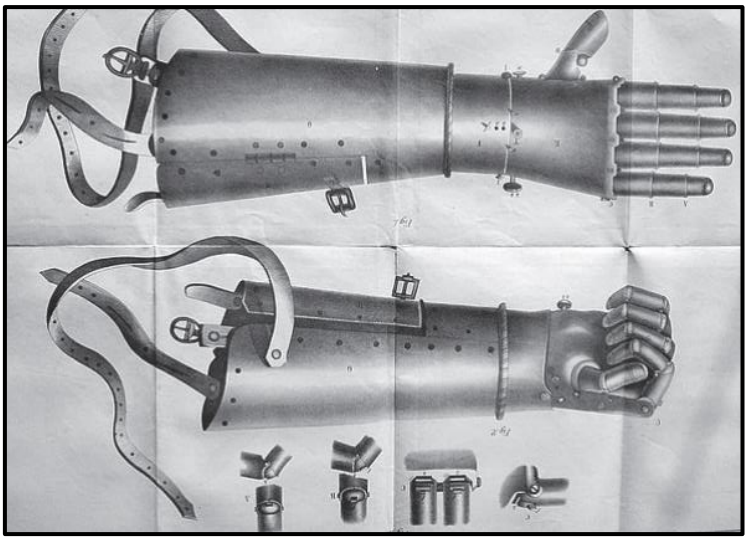

Figure 1 - Gotz von Berlichigen Prosthesis [3]

2.1.1. Types of Upper Limb Prothesis

The upper limb prosthetic devices fall into five categories, passive, body-powered, myoelectric, hybrid and activity-specific prosthetic [5], [6].

The passive prosthetics hands are the simplest of the five, since they do not involve any type of mechanisms to power its movement. Is necessary for the user to morph the device according to their needs. These can also be static having only aesthetic purposes [7]. In the work of Dechev et al. a prosthetic hand was developed, that has the capability of a passive adaptive grasp, this device can be observe on figure 3 (A) [8]. In a more commercial approach, an example of this device is the Ottobock 8K19 spring-loaded thumb System Hand that can be observe in figure 2 (B) [9].

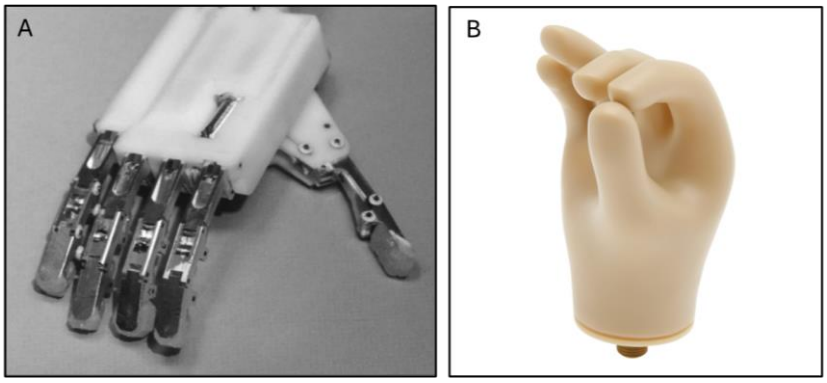

Figure 2 - Passive prosthetic hand (A) from Dechev et al. (B) from Ottobock.

Body-powered prothesis (BPPs) are controlled by adjusting the tension of cables or a lever system to close or open the device, that can be total ((figure 3 (A)) or partial (figure 3 (B)). The benefits of BPPs are the moderated cost, a small training period, easy to repair, having a low weight and being simple to operate. Additionally, by voluntary closing the prothesis, the user is provided with enhanced physiological proprioception, and it increases the proprioceptive response to tool the user may interact with. Examples of BPPs are the Hosmer work hook shown on figure 3 (A), the partial finger replacement from Art Dynamics in figure 3 (B) and the TRS Grip in figure 3 (C) [10], [11], [12], [13].

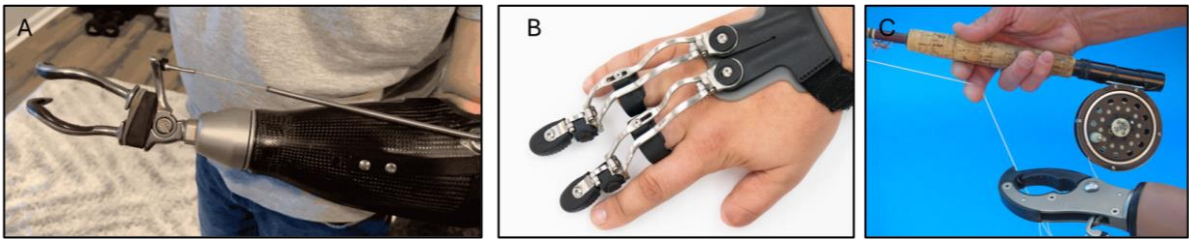

Figure 3 - Body-powered prothesis (A) Hosmer hook [12] *(B) partial finger replacement* [11], [12] (C) TRS Grip[10]

The myoelectric prothesis are a more advanced approach in hand replacement devices. The movement of the hand is powered by electrical actuators, that are controlled by reading myoelectric signals on the user forearm or arm. To achieve this kind of human-machine interface, is necessary to use electrodes on the system for gathering the raw data, and a machine learning algorithm embedded in the electronics, that classifies the electromyography signals into gestures. The system will then give an order to activate the actuators closing, opening or executing a gesture that the code recognises [14], [15], [16], [17]. Some examples of this type of device are the be bionic hand from Ottobock, shown on figure 4 (A), commonly known for its advanced technology and the ability to execute various grip patterns [18]; the Michelangelo hand also from Ottobock, shown in figure 4 (B), that has a more natural motion and human like appearance due to the covering, offering a range of multiple grip patterns [19]; the I-Limb Quantum, a prothesis from Össurs built in titanium and also capable of multiple grip patterns, shown in figure 4 (C) [20].

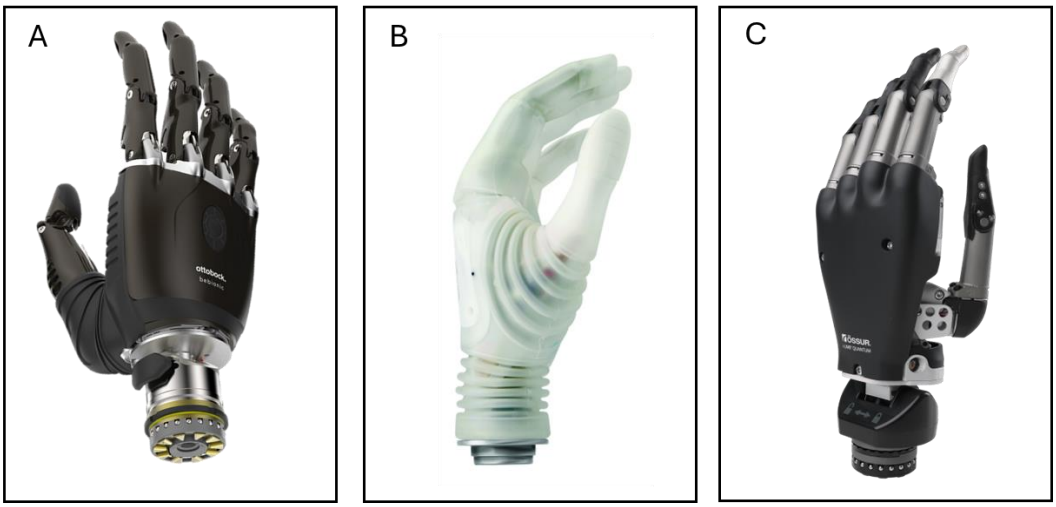

Figure 4 - Myoelectric hand prothesis (A) be bionic [18] *(B) Michelangelo hand* [19] *(C) I-Limb quantum*[20].

A hybrid prothesis is simply the combination of different methods of actuation in one device with the intuit to improve its performance [1]. An example of this type of device can be seen on the work of Castro et al. where a prosthetic hand prototype was developed, shown on figure 5 (A), that integrated a myoelectric actuation system with computer vision that recognise an object and defines the pattern to grasp it [21]. In figure 5 (B) it's possible to observe a partial hybrid hand prothesis from Arm Dynamics with a body-powered index and thumb due to the existence of this residual body parts, that is combined with three passive fingers [22]. The most frequently utilized hybrid setup combines a body-powered elbow with electric powered hand and wrist, this configuration can be seen in figure 5 (C) [1].

Figure 5 - Hybrid prothesis(A) from the work of Castro et al [21]*(B) partial hand design* [22] *(C) full arm* [1].

The activity-specific prosthetics are apparatus created for a specific activity or job where BPPs, myoelectric or passive devices could be damaged or not displaying a good performance [1]. Some examples of this devices are shown on figure 6, where figure 6 (A) is specific for fishing activities, figure 6 (B) for working with wood, figure 6 (C) for climbing and figure 6 (D) for playing drums[23].

Figure 6 - Activity-specific prothesis (A) for fishing (B) for work with wood (C) for climbing (D) for playing drums [23].

2.1.2. Existing Solutions

The literature includes various studies in this field aimed at recreating a substitute for the lost limb using different approaches.

Tabassum et al. (2017) developed a low-cost prosthetic hand using an Arduino board and MG995 servo motors. They achieved independent movement for each finger, having five grip patterns. This prototype could be implemented in transradial prothesis, but other suggested applications were in aerospace, mining and manufacturing industries. In these cases, the model would be incorporated into a robot [24].

Zappatore et al. (2017) show a prosthetic hand system that only required one DC motor to function. In order to power hand motion, multiple differentials in serial and parallel configurations were used, allowing the hand to adapt to the object. The model is named ADAM's hand and can achieve 15 degrees of freedom with just 1 degree of actuation. In figure 7 (A) it is possible to see the internal structure of the system [25].

Vanhuy et al. (2015) combined a hand designed in Solid Works and 3D printing with MG995 servo motors for actuation. The control system is composed of an Arduino Uno and flex force sensors incorporated in a glove. These are sensors that when bended change their resistance. With this variation is possible to map the position of the servo. In figure 7 (B) is possible to observe the assembled model and all their components [26].

Dunai et al. (2021) created a prosthetic hand that emulates the human hand with its phalanges and metacarpal bones, and soft joints. The joints allow for a high level of movement and degree of freedom. The hand is actuated by five stepper motors connected to a string and the thumb abduction/adduction was mediated via a servo motor SG90. To control the pressure applied by the device a feedback system was created using force resistive sensors (FSR). Surface Electromyogram Myware sensors were used to allow the classification of the hand movements. To control the system, an Arduino Mega board was used. Figure 7 (C) shows the model obtain in the work [27].

In the work of Pitou et al. (2018) a different approach was made to the surface electromyography. Due to their work having a focus on creating a low-cost prothesis for developing countries gel electrodes are not an option because they are not reusable. The researchers used embroidered textile electrodes (figure 7 (D) (d1)) and run sEMG experiments in south Africa. The electrodes were placed on the forearm of three amputees, shown in figure 7 (D) (d2). The result obtained were compared with gel electrodes. The gel electrode shown an accuracy of 97.22 %, while the textile ones show 93,73%. Despite the low accuracy for the embroidered electrodes the performance is high. The model of the prosthetic hand develop in this work is shown in figure 7 (D) (d3) [28].

Lanigan et al. (2017) developed a 3D functional hand actuated by MG995 servo motors situated in the forearm and controlled by an Arduino Mega (figure 7 (E) (e1)). The model has the capability to grab multiple day to day objects as shown in figure 7 (E) (e2). The fingertip of each finger has an embedded thermistor and a force resistive sensor. These serve to give feedback to the user of the temperature of the grabbed object and how much pressure is applied by the motors. In figure 7 (E) (e3) it's possible to observer the fingertip configuration and how the two sensors are accommodated [29].

In the work on Morales el al. (2017) a MYO armband was used to acquire the myoelectric signal of the forearm, to train machine learning (ML) algorithms. Five gestures/movements were recorded: hand flexed inwards, hand flexed out, close hand, spread fingers, and relax position. From this data, multiple features were extracted such as root mean square (RMS), mean absolute values (MAV), number zero crossing (NZC) and others. Two classifiers were trained a feedforward neural network (FNN) and support vector machine (SVM). To measure the accuracy of the ML algorithms k-fold cross validation was applied. The SVM shown the better performance, and the best feature is the combination of MAV, RMS, VAR and standard deviation (STD) having an 92% accuracy [30].

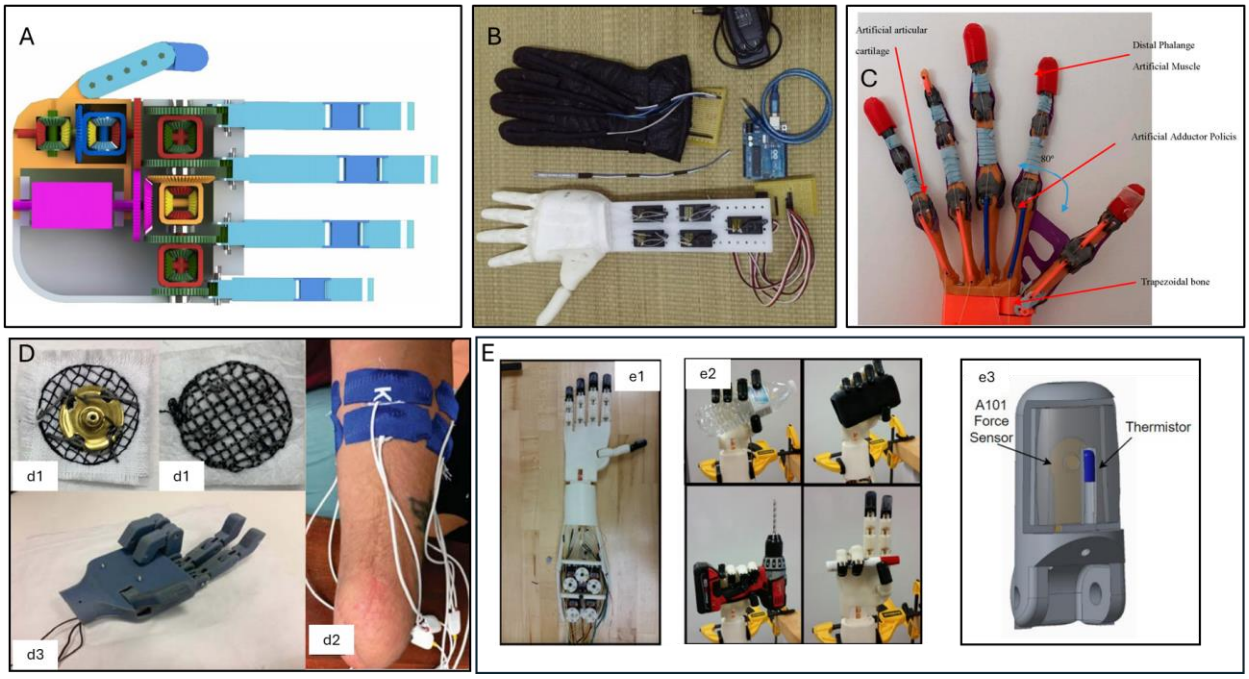

Figure 7 - Work of (A) Zappatore et al. (2017) (B) Vanhuy et al. (2015) (C) Dunai et al. (2021) (D) Pitou et al. (2018) (d1) textile electrodes (d2) electrode placement (d3) hand model (E) Lanigan et al. (2017) (e1) assembled model (e2) grabbing test (e3) fingertip design.

2.2. Manufacturing Method

The manufacture of prosthesis can be performed by two different methods, conventional methods, and the additive manufacturing methods. As the name indicates, the first one resorts to more conventional manufacturing methodologies (usually subtractive), while the second adopts more technological and recent methods [31], [32].

The conventional manufacturing methods requires the creation of several moulds of the pathologically affected part for the socket creation. This process is time consuming and uncomfortable as it is necessary to apply plaster on the residual limb and wait for it to solidify. If it does not meet the necessary requirements, the process must be repeated. Another disadvantage is that a person with a mobility problem must travel to the production site, as it is not efficient to bring all this working material to the patient's home [31], [32].

Regarding additive methods, as already mentioned, they use the most current technologies and adopts CAD and 3D printing methodologies. In contrast to the initial of conventional process, initially a scanner or computer tomography is used to capture the residual limb and generate a three-dimensional digital twin. With it, is possible to start working directly on the digital model, using CAD/CAM software. In the case of a prosthesis, this process can be applied to produce the socket in the stump. To produce the prosthetic device, it is possible to apply this method to model all the components to make a final product as optimised as possible. With this technology it is possible to obtain unique geometry that could not be obtained by traditional processes. The additive manufacturing process not only acts in polymers, but it also allows the use of various materials such as ceramics and metals. With metals it is possible to obtain fully customized implants to each patient, using imaging. This method can give the patient a cheaper and viable way to get access to these types of devices [31], [32], [33].

Additive Manufacturing is a process based on 3D digital design and adding material layer by layer to create a unified model. This process has three main steps that work together to produce custom and with complex parts. These steps are a) model creation using CAD (computer-aided design) software, b) converting the 3D model to G code (Geometric Code), and c) the printing process [34].

To create the design is necessary to use a CAD software, where the user have multiple tools to use allowing him to create and manipulate a 3D digital model with high level of detail. These programs allow to articulate parts to simulate their behaviour and by finite element analysis understand how the model structure will behave when expose to external forces. This allows to analyse how the forces will affect the model and what parts will be more stressed, serving as information for viability of the structure in their function and where material can be

removed because is not contributing to the structural strength, creating a more optimized component [34], [35].

Since the 3D printers read G code, a common language for CNC (computer numerical control) machines giving the information to the printer where and what to do. The CAM software works as a link between the CAD and the 3D printer, by slicing the model in layers and allowing the user to define parameter for the printer. The thickness of layers, the speed of the printing process, the temperature of the bed and the nozzle, type of filling design and wall thickness, these are all variables that can be customized in function of the type of part that will be printed and what material will be used [34].

2.2.1. 3D Printing

With the advance of the technology, more sophisticated manufacturing methods were developed, allowing the use of more and different materials, creating even more detailed parts in different fields, biomedical, aeronautical, and industrial sectors. This section makes an approach to 3D printing focusing on the method applied on this work [36].

The fused filament fabrication (FFF) uses a thermoplastic polymer filament that is heated by the nozzle, extruded to the printer bed and deposited on top of the previously layer, fusing layer with layer. This process can be seen on the figure 8. The mechanical properties of the model are affected by the parameter defined on the CAM software. The most commonly used polymer is PLA, but ABS (acrylonitrile butadiene styrene), PEEK, (polyether ester ketone) or TPE (thermoplastic elastomer) are other options available on the market. This process has a low cost due to the cheap and common materials, is simple to used and accessible but require an extra finishing after the printing process because of the poor surface resolution [37].

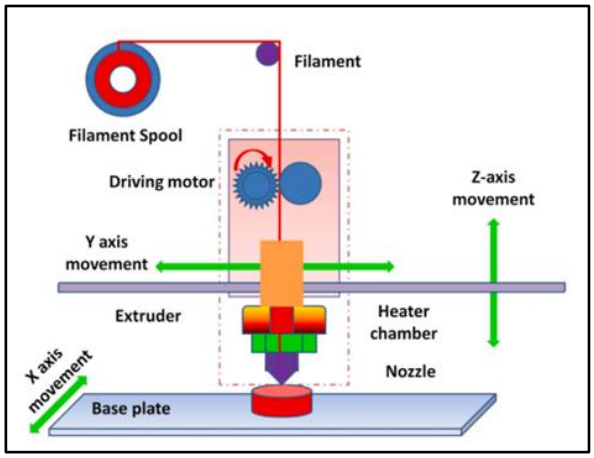

Figure 8 - FFF schematics.[37]

2.3. Electronics Components

This sub-chapter make an approach to the main electronic parts used in the creation of prosthetic hand.

Microcontrollers

The Arduino is a simple open platform for creating electronic projects, it's composed of two parts, the hardware and the software.

The hardware component, the microcontroller, exists in different sizes that fits all kind of different projects. The three most common are the Arduino nano, Uno and Mega (figure 9), they differ not only in size but also in functionality. The Nano offers a small size, a cheaper price, has an Atmega328 processor with 16Mhz, has 32Kb of memory and 2Kb of RAM, includes 14 digital and 6 analogue pins [38]. The Uno has the same features but has a larger PCB and don't require to be place on a breadboard for prototyping because contains built in rails to connect jumper wires [39]. Finally, the Mega has the largest size, a different processor, ATmega2560. but also, with 16Mhz, a memory of 256Kb, 8Kb of RAM, 16 analogue pins and 54 digital pins [40], [41], [42].

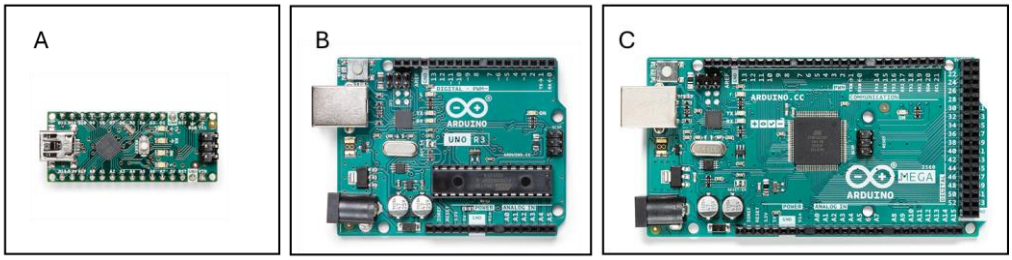

Figure 9 - Arduíno (A)Nano [38] *(B)Uno* [39] *(C)Mega* [40]

These boards can light up LEDs, control motors, receive signals from sensors and button inputs, which allow them to be used in thousands of different applications. To control all these functions, a program needs to be coded. This will dictate how, when and where to send or process information. The free software Arduino IDE allows to program the board in the best way possible to execute the desired functions and uses C++ language [43], [44]. These boards can perform Inter-Integrate Circuit (I2C) that is a serial communication protocol that allow the Arduinos to communicate with each other or with another device that support this communication. The information trade-off is made via the Serial Data Line (SDA) and the Serial Clock Line (SCL) pins. All the devices are connected to these pins, and each have a special

address. When information is sent through all the devices receive it but only the one with the correct address executes it [41], [42], [45].

Sensors

The two physical quantities that are necessary to measure in the prototype are force and temperature.

For temperature sensors the most suitable are thermistors or IC temperature sensors, due to their small size. Thermistors are a type of electronic component were their resistance change with temperature. There are two classes the negative temperature coefficient (NTC) where the resistance drops with the increasing temperature (figure 10 (A)) and the positive coefficient (PTC) thermistors where the resistance increases with the temperature (figure 10 (B)) [46], [47].

IC temperature sensors are semiconductor devices that don't require external accommodation, are simple to use and have a low cost [48]. LM35 (figure 10 (C)) is an example of these type of sensor, have three connection points, one for power, one for ground and the other for output voltage (Vout). This is a linear sensor, the incrementation on Vout is 10 mV per Celsius degree [49].

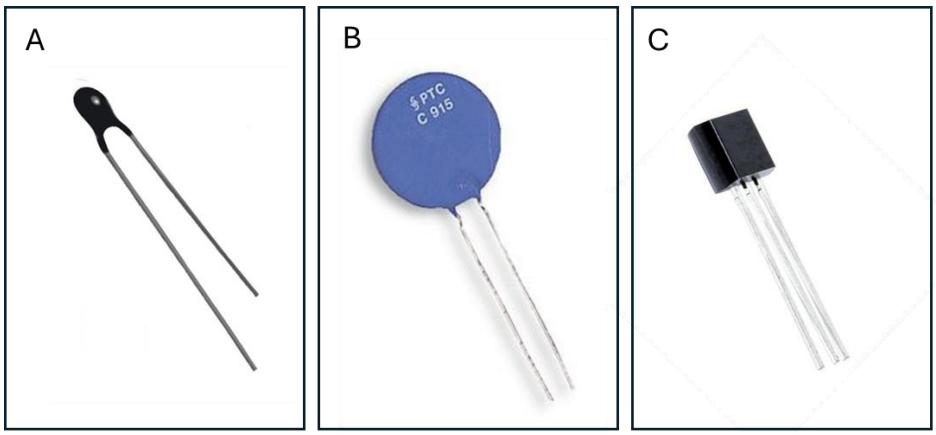

Figure 10 - Temperature sensors (A) NTC thermistor [50]*(B) PTC thermistor*[51] *(C) LM35*[52].

The market has different types of force sensors, the ones that this work focus on are piezoresistive force sensors. These components change their electrical resistance when a load is applied. This variation is detected via semiconductor material in the interior of the sensor [53]. The FlexiForce line from Tekscan, offers a range of sensors with different sizes (figure 11(A)) [54], [55]. The A101 (figure 11 (B)) is smallest having 15,6 mm of length and 7,6 mm of height, the sensing area has a circular area with 3.8 mm of diameter. The difference in size when compared to the rest of the sensor can be seen on figure 11 (A) [56].

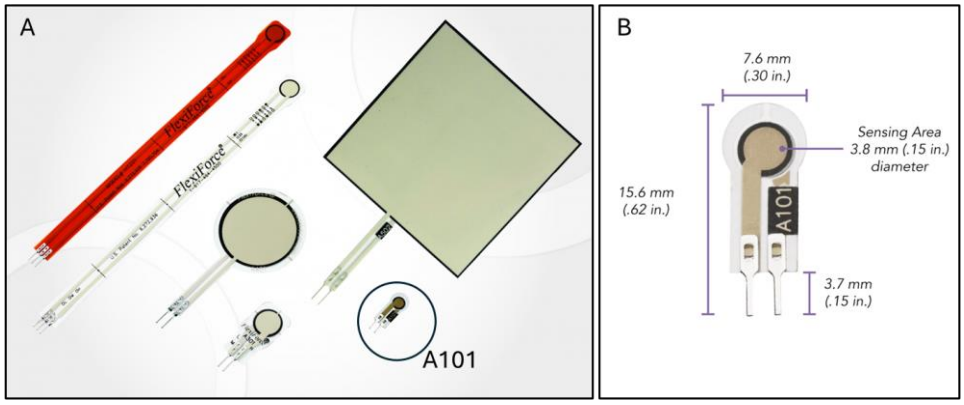

Figure 11 - Force sensors (A) Tekscan force sensors[55] *(B) A101 force sensor*[56].

Actuators

The actuation system is a crucial component when develop a prosthetic hand because is responsible for all the movements of the model. Servo motors are a low-cost option for an actuation system and have a high precision [57].

The SG90 is a small motor, having only 1.8Kg per cm of torque (figure 12 (A)) [58]. This device serves the purpose of controlling the position of the thumb in the works of Dunai et al. and Lanigan et al., due to its size can fit inside the hand [29], [59].

The MG995 its larger and has a higher torque of 10Kg per cm and uses metal gears (figure 12 (B)), instead of plastic ones [60]. In the literature, normally serve the purpose of actuation the finger, (closing and opening the hand). Because of their size, they sit on the forearm of the model. In the work Koudelkova et al. (2023) five of these motors were used on the forearm, to actuate the fingers by pulling a string [61].

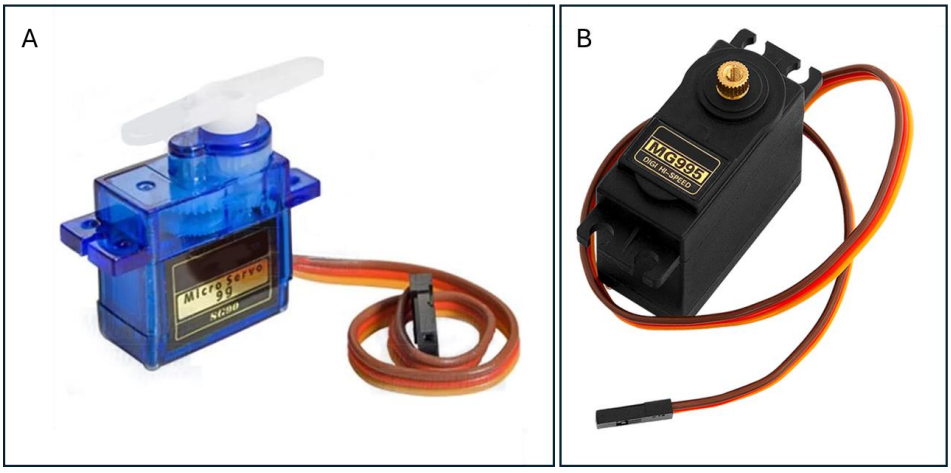

Figure 12 - Servo Motor (A) Sg90 [62]*(B) Mg995* [63].

2.4. Myo Armband

Myo is a wearable armband created by Thalmic Labs and can be observed in figure 13. That enables gesture-based control of various connected devices like PCs, gaming consoles, and robots. By detecting myoelectric signal in the forearm. It's composed of eight sEMG electrodes, a gyroscope, accelerometer and a magnetometer [30], [64], [65].

In the work of Moura et al. (2016) a myoelectric signal processing and analysing interface was developed. The system has the ability to plot and read sEMG raw data from MYO, extract feature from the signals and is also able to classify them [66]. Cognolato et al. (2018) investigate MYO's own classifier capabilities in gesture recognition of transradial amputees. The three subjects elected executed a sequence of gestures. The data was acquired via Bluetooth and process with MYO SDK [67]. Hussain et al. (2020) used the MYO for the recognition of fourteen gestures. The data was classified with Multi-layer Perceptron Neural Network having an average accuracy of 90,5% [68].

Figure 13 - Myo Armband [65].

2.5. Machine Learning

Machine Learning is a part of artificial intelligence (AI) that focuses on algorithms with the capability of learn and make predictions from data. This branch of AI allows machines to recognize patterns a create relationships in the data [69], [70], [71].

Four types of machine learning techniques are normally considered, namely a) supervised, b) unsupervised, c) reinforcement and d) semi-supervised learning. Supervised learning algorithms learn from labelled data, focus on classification and regression. In unsupervised learning the algorithms use unlabelled data to learn. K-mean clustering and hierarchical clustering are some examples of models with unsupervised learning. Semi-supervised learning is a ML technique where the model learns from combined data, label and unlabelled. Reinforcement learning the model are created on penalty or reward system [71].

The ML models used in this work were artificial neural networks (ANN) and support vector machine (SVM). Their choice was based on previous works, that used these algorithms for gesture recognition [30], [72].

Neural Networks (NN) are a group of ML algorithms that are based on the human brain's structure. They have layers of nodes or neurons that are interlinked, each link is associated with a weight and as bias. The NN learn by adjusting these weights and bias based on the data that they are fed. The error in their predictions is used to adjust the weight values using backpropagation algorithms. A NN model is compose mainly by the input layer, hidden layers and the output layers, the schematic that show this structure com be seen on figure 14. In the input layers the neurons receive the raw data. The hidden layers are intermediary and are situated between the output and input layers. Their number change with complexity of the model and the problem to be solved. The output layer is the final one and is the prediction or output of the neural network [71], [73], [74].

These systems offer a high flexibility and can created complex relationships in the data and have application on speech recognition, image and text classification [74].

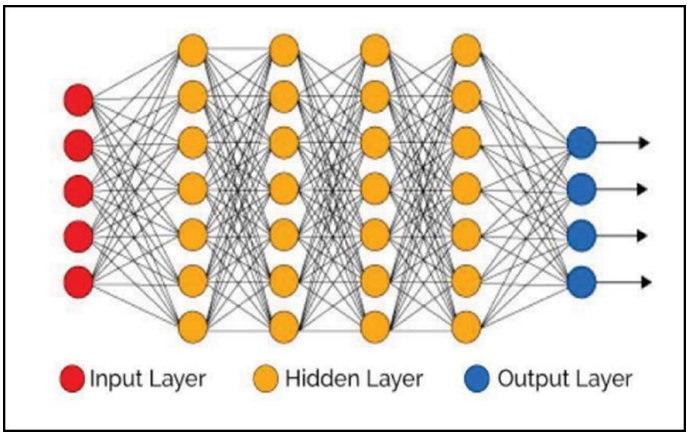

Figure 14 - Neural network structure[74].

Support vector machines (SVMs) are supervised learning algorithms used for classification. The main principle of the model is to find the optimal hyperplane that split the data point of different classes in the best way possible, having a maximum margin between them. The data point that are close to the hyperplane are maned support vectors and help define the boundary. The hyperplane can be observed in figure 15. SVMs models are normally used for in text classification [75], [76], [77].

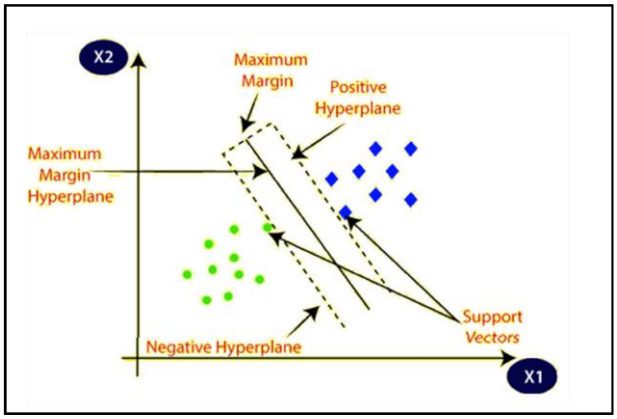

Figure 15 - SVM hyperplane[76]

Chapter 3 - Materials and Methods

This chapter explains all the methods and material used to achieve the main objective of this work, how the design thinking was applied on the creation of the model, passing through different development stages that allow to create a more polished and functional product.

3.1. Materials

Polylactic Acid (PLA) filament was used for the hand 3D prototype, a Prusa Mini Plus an Any Cubic Kobre 2 Pro for printing. The jumper wires used to produce all the hand components, Arduinos, OpAmps, capacitators, breadboards, resistors, Peck Tech 4390 multimeter and the power bench supply were provided by the EST Setúbal. The LM35 and flexiforce A101 sensors were bought from Digi-Key Electronics. The servo motor SG90, joysticks were acquired Robert Mauser Lda, the servo motors MG995 acquired from Az-Delivery, the silicone, the string and the rubber bands were bought in a conventional retail store.

3.2. Prosthetic Hand Design

This section explain what methods were used in the design of the prosthetic hand, englobing the sketching, CAD and 3D printing methodologies.

3.2.1. Initial Sketches

This is a crucial step in the design process, it allowed to quickly visualize ideas, experiment with concepts, and identify potential challenges before committing to CAD. The sketches were made on paper and define the based for the component to be created in Fusion 360. First a sketch from the skeleton of the hand was created. The next step was to sketch the articulation point and different finger designs. Finally, the design of the fingertips was created.

3.2.2. Computer-Aided Design

The all component in this work were designed using the software Fusion 360. Three finger models were designed, model A and B were already defined in the sketch section, while the third one, model C, appears due to practical prototyping. After these components the hand, thumb and forearm were designed. To support and store the electronic components a box was created. The components that are based on the initial sketches, but some will suffer alteration due to the better understanding of the models and their behaviour when articulated given by the three-dimensional view of the software and to testing the prototypes.

3.3. 3D Printing Process

The printing process was done by a Prusa Mini+ and by an Any Cubic Kobra 2 Pro, all part were printed in PLA. The settings differ between the two printers, the parameters used for each printer are represented on table 1. Due to the Prusa having a small printing volume of 180x180x180 mm [78], and a lower printing speed was charged with small parts. The Kobra 2 Pro because has a larger printing volume of 220x220x250 mm [79] and a higher printing speed was charged with larger parts such as forearm and the box. The high speed allows to use a small layer thickness having better surface quality.

Table 1 - Printing parameters used

Printer	Layer thickness (mm)	Infill (Type)	Infill (%)	Printing Speed Used (mm/s)	Max Printing Speed (mm/s)
Prusa Mini+	0.4	Gyroid	15	80	200 [78]
Kobre 2 Pro	0.2	Gyroid	20	230	500 [79]

3.4. Actuation Tests

This section explains how the tests for the finger actuation were carried out to define the better servo motor and which model perform better. These will allow to create an optimized finger actuation system.

3.4.1. Auxiliar components

To analyse the behaviour of the models when actuated by the different motors, it was necessary to develop a system to test them in the same conditions. To achieve this, auxiliar components were created to secure the fingers and the motors in the same place. This allows to actuate de fingers conveying mechanical energy from the actuator to the strings without any loss. A base to secure the finger was created alongside a system of modular components that can be add to the base that support the fingers and motors. All of these were designed in Fusion 360 and 3D printed.

3.4.2. Fingers Actuation Tests

For these tests the three models (A, B and C) were secured in the base and attached to the respective servo system, these were activated to the maximum amplitude at the same time, in total were carried out three tests, testing all models with each motor system. The motors were controlled by an Arduino that receives the input control from a joystick. In figure 16 can be observe the tests apparatus, figure 16 (A) shows the assembly for test with a single SG90, figure 16 (B) exhibit the tests with the double SG90 system and figure 16 (C) display the test using the MG995s.

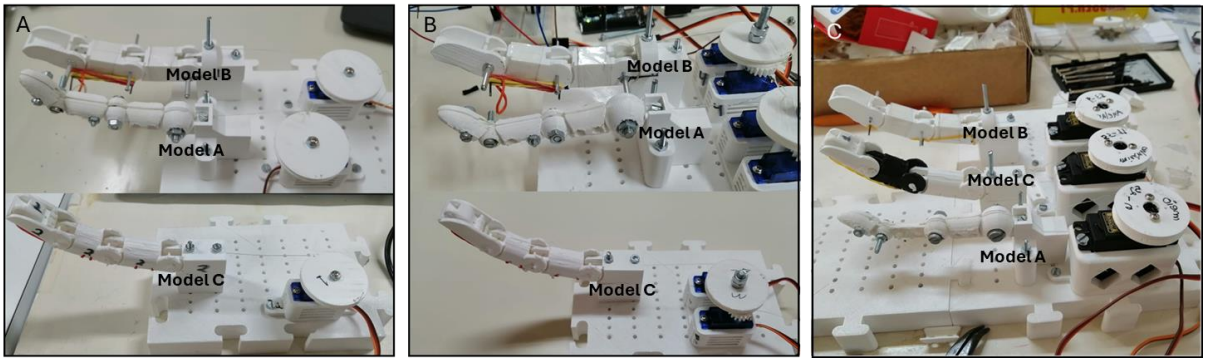

Figure 16 - Finger actuation tests (A) with single SG90 system (B) with double SG90 system (C) with MG995 servos

3.4.3. Thumb Actuation Test

The thumb was tested in two ways, one for the abduction/adduction and the second to the flexion and extension. For this the microcontroller receives a second input control from the second channel of the joystick to control abduction/adduction created by the SG90 inside the hand, highlighted in red in figure 17 (A). For the flexion and extension, an MG995 servo motor

was used, placed in the forearm. By this point in the work, it had already been established that the MG995 motors would be used (figure 17 (B)).

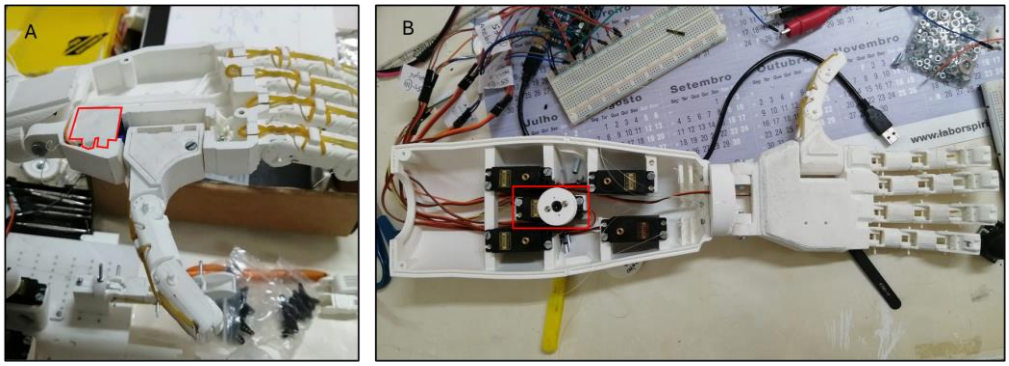

Figure 17 - Thumb testing (A) SG90 position (B) MG995 position

3.5. Electronic and Sensory Component

The electronic system has the main function of controlling the hand movements according to sEMG signals and to sense the object temperature and applied pressure on it. In this phase of the work were established five modules that compose the electronic and sensory component, namely, the sensory module, multiplexing module, the control system module (microcontrollers), actuator module and the user interface module. This section show all the methodolgies used to assembled, calibrate and test all the different modules.

3.5.1. Sensory Module

This consists in two types of sensors the LM35 temperature sensor and the A101 pressure sensor. Firstly, the sensors signals were conditioned, the sensors were calibrated and finally tested.

Pressure Sensor Signal Condition

The A101Fflexiforce requires an electronic circuit to convert resistance variations into an amplified voltage. The circuit implemented it's an active low pass filter provided in the sensor datasheet and is represented in figure 18 (A). An operational amplifier MCP6004, provide a gain in the filter passband, and above the cutoff frequency the circuit provides an attenuation of -20dB/decade since it's a first order filter. The equations of the circuit are represented in the following equation.

$$V_0 = -\left(\frac{R_f}{Rs}\right).\left[\frac{w_0}{s+w_0}\right].V_D[\text{V}] \quad \text{(eq1)} \qquad w_0 = \frac{1}{R_f.C}[\text{Hz}] \quad \text{(eq2)}$$

Where R_s represents the A101 resistance, R_f the feedback resistor (100kΩ), responsible for defining the amplifier gain and one 47 pF capacitor for defining the filter cut-off frequency (w_0).

Temperature Sensor Signal Condition

The LM35 it's a temperature sensor with a built-in amplification circuit, so it requires the power and ground of the circuit (figure 18 (B)).

The equations 3 and 4 are used in the microcontroller to convert the ADC output values from LSB number (nLSB) to voltage values and to convert voltage to temperature in Celsius, respectively.

$$V = \frac{5.0}{1023} * nLSB \quad [\text{V}] \quad \text{(eq3)} \qquad T = \frac{V}{0.01} \quad [^{o}\text{C}] \quad \text{(eq4)}$$

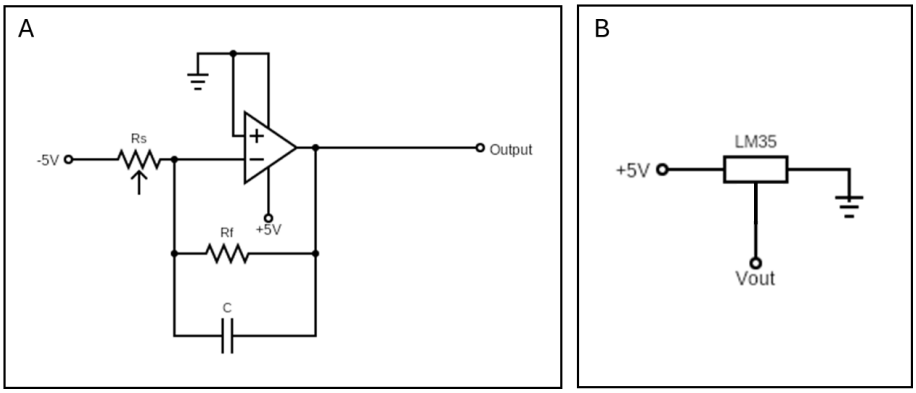

Figure 18 – Electronic schematic (A) from Flexiforce A101 (B) from Lm35.

Pressure Sensor Calibration

To test the A101 is imperative to stabilize the system to concentrate the applied force on the sensor for this A loading cell was designed. It is composed of two components, the base and the platform. The FlexiForce sensor was calibrated using a series of marked weights. The sensor was securely mounted onto loading cell, and the weights were placed on the loading platform to concentrate the force directly at the center of the A101 sensor.

Temperature Sensor Calibration

For the calibration of the LM35 temperature sensor, an external thermometer (Xiaomi Mi LYWSD03MMC) was used to validate the temperature readings from the Arduino. This process helped to identify and correct any potential errors in the measurements.

In the subsequent experiment, two LM35 sensors—one standard and one coated with silicon—were placed inside the test setup's fingers, positioned 4 cm away from a constant heat source maintained at 300ºC. Temperature readings for both sensors were recorded at 30-second intervals over a total test duration of 25 minutes.

Pressure Sensor Testing

Connecting the A101 to the Arduino to establish a feedback system enabled the implementation of a mechanism to limit the pressure applied by the hand on an object. This mechanism was hardware-implemented using a potentiometer, with the output voltage determining the maximum force to be applied. The figure 19 (A) illustrates the test circuit of the feedback system. In this system the analogue voltage output from the A101 sensor amplifier and the variable voltage threshold, adjusted via the potentiometer (R1) were connected to the microcontroller's ADC ports. Additionaly, the motor control used the PWM output ports.

For testing the LM35 a small electronic circuit with three LEDs (green, yellow and red) and active buzzer, was built with all connected to Arduino (figure 19 (B)). If the average temperature is below 35 ºC, the green led turns on, if it is between 35ºC and 50 ºC, the yellow turns on, and if it exceeds 50ºC red turns on and the buzzer is also activated.

The temperature test was conducted using a soldering iron with a constant temperature of 300ºC placed 1cm away from each LM35 and a commercial thermometer. This setup evaluated the sensor's response and validated its accuracy against the reference thermometer.

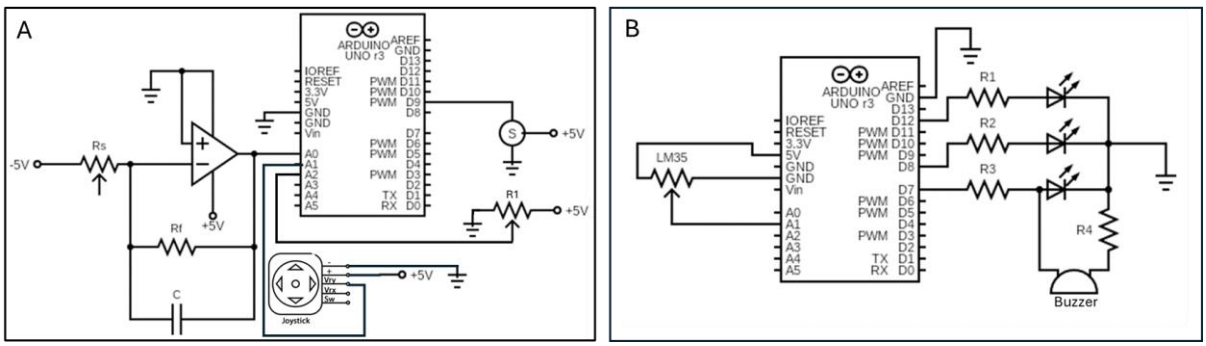

Figure 19 - Testing circuit (A) for A101 (B) for LM35

Fingertip Assembly

After testing the sensors, it was necessary to integrate them into the model. Both LM35 and A101 were place inside a distal phalange of each finger. To achieve this, a process with four steps was created. This can be observed in figure 20, starting on figure 20 (A) and finishing on figure 20 (D). The distal phalange was fixed inside of the base component of the loading cell, and the lower part of modular component with the sensors in their respective place was added (figure 20 (A)). In the next the modular component's upper part is added separating the two sensor (figure 20 (B)). A layer of silicone is added (figure 20 (C)), with help of a wet spatula and the fingertips were left to dry for a week.

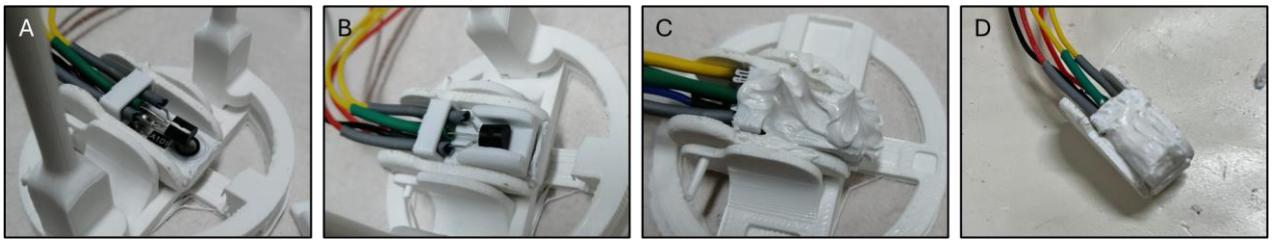

Figure 20 - Process for sensor encapsulation (A) step 1 (B) step 2 (C) step 3 (D) step 4.

3.5.2. Multiplexing Module

To better evaluate the performance of the multiplexing task, two tests were conducted. The first, called the *Function Test* aimed to verify the relation between the MUX select pins and the routing of a specific input to the output. The second test, called *Multi-Sampling Test* has intended to find the minimum sampling period required between two MUX inputs. The objective was to optimize the sampling period for each sensor while ensuring accurate readings. The minimum sampling time corresponds to the period needed for the sampling signal to stabilize after switching between channels.

The Function Test

This test was conducted using a breadboard (solderless board) and consisted in applying different pre-defined voltages values to the input pins of the MUX. The voltages were routed to the output by selecting the appropriate combinations on the A pins (figure 21). The test allowed a comparison between the input and output and calculate the relative error (eq 5) and absolute error (eq 6) using the equations below.

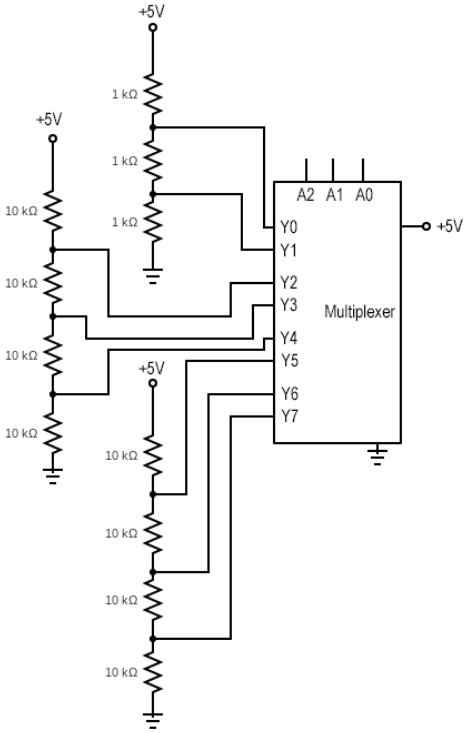

Figure 21 - MUX functions test apparatus.

$$Absolute\ Error = |Y_{in} - Z_{out}| \quad \text{(eq 5)} \quad Relative\ Error = \frac{Absolute\ Error}{Z_{out}} * 100 \quad \text{(eq 6)}$$

The Multi-sampling Test

For this test, the setup was adapted from the previous test, but the process was no longer manual. Instead, it was automated to operate continuously and periodically. The main purpose was to evaluate the highest possible frame rate, while allowing the signal to stabilize at the MUX output.

The Arduino controlled the reading of the Z output and the switching between the Y ports. Every five seconds the Y channel was changed, and the corresponding Z values were recorded in a csv file using a software tool called CoolTerm which functions similarly to the Arduino IDE's serial monitor in Arduino IDE but allow to export the data to a text file with comma-separated values (CSV format).

3.5.3. User Interface Module

This module consists of four parts: the displays, pressure voltage limiter, servo control and temperature alarm system. Each system was individually tested to ensure proper functionality.

The displays were powered and connected to Arduino to print a small phrase, “Hello World”, to verify that all pixels were functioning correctly. The pressure voltage limiter, as previously described, is a potentiometer. To test its functionality, the device was powered, and the middle pin was connected to the voltmeter to confirm that the voltage values changed when the knob was turned. The servo control module includes two joysticks. To test their performance, the X and Y channels were connected to the microcontroller ADC and the output values were monitored to check if the values were changing as expected. Finally, the temperature alarm system, as described before, is composed of three LEDs and an active buzzer. These components were powered and tested to check if everything was working.

3.5.4. Actuator Module

This module consists of the hand and forearm system, including the servo motors, create the actuation system for the prosthetic. All servo motors were powered on, connected to Arduino and the rotated 180 degrees to verify if they operated ad intended, figure 22 (A) shown the schematic for the circuit.

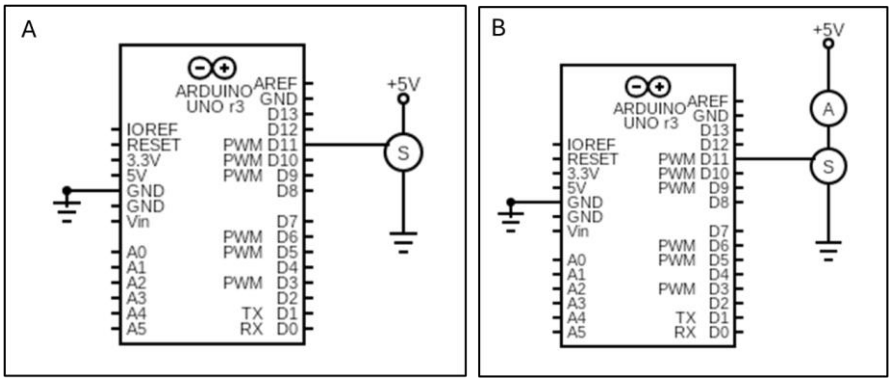

Figure 22 - MG995 working test circuit.

To create an appropriate power supply for the system, it is important to know the current consumption, and the servos are the primary components responsible for consuming the most current. Therefore, an amperemeter was used to measure the current drawn (figure 22 (B)). The MG995 was fixed inside the forearm and hand system, and three test were conducted by varying the object against which the finger applied force. The tests were performed as follows: first, without any object; second, with an empty can; and third, with a spatula. These tests were repeated, but this time, wires for the sensor were inserted inside the finger, to evaluate the changes in current consumption. In total, six tests were carried out. The table 2 summarizes all the test results.

Table 2 - MG995 current drawn test apparatus summary.

Test name	Holding object	Wiring	Object
Mg1	No	No	-
Mg2	No	Yes	-
Mg3	Yes	No	Empty can
Mg4	Yes	Yes	Empty can
Mg5	Yes	No	Spatula
Mg6	Yes	Yes	Spatula

3.5.5. Control System Module

The control system module consists of two Arduinos with different purposes. The first one, Arduin 1, receives the data from the pressure sensors and controls its respective MUX, also controls the opening and closing of the fingers and the adduction and abduction of the thumb. The second one, Arduino 2 is responsible for receive the data from the temperature sensor and control its respective MUX, controls the alarm system, and rotation of the forearm. To execute all of these functions a code was implemented in the microcontroller using C++ languages.

3.6. Wiring Accommodation and Model assemble

After testing and calibrate the model components, the next step was the assembly part. The forearm was securely attached to the cover of box housing the electronic components. The sensor wiring was pass through the fingers (figure 23 (A)), to the wrist (figure 23 (B)), behind the servos in forearm (figure 23 (C)) and finally connected to electronic components (figure 23 (D)).

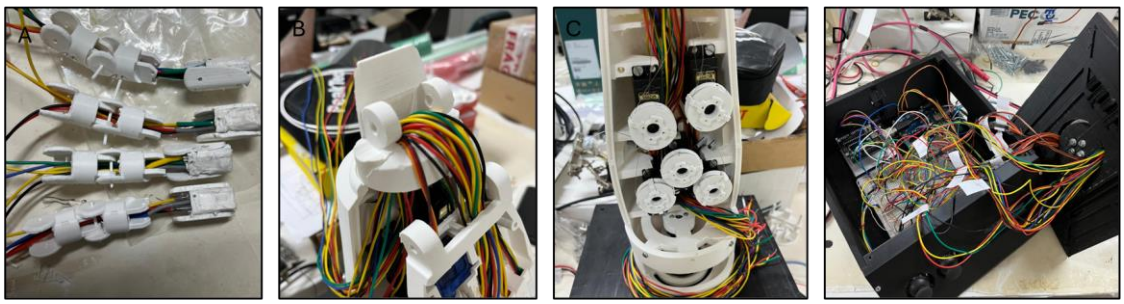

Figure 23 - Wiring accommodation in (A) the fingers (B) the writs (C) in the forearm (D) the box.

After integrating the wiring into the system, the complete model was assembled. The box cover was secured with screws and the wrist was attached to the hand.

After assembly, the model executed five predefined gestures, which can be changed by pushing the joystick button. The system also can be controlled manually using the joysticks. The selection of these gesture will be discussed in the next chapter. Additionally, the model was tested in holding different everyday objects to analyse the behaviour of the actuation system. The objects chosen were aligned with those used in the work of Lanigan et al. (2017) due to the similarities between the two models.

3.7. AI Based Control

In addition to manual control of the prosthetic hand, this thesis also aimed to develop an artificial intelligence-based control system using sEMG signals. A pre-defined set of key gestures was selected to train machine learning (ML) algorithms for gesture recognition.

The recording of myoelectric dataset is essential for training the ML algorithms. Proper annotation of the data, including event segmentation and classification, enables a supervised training process where the algorithms learn from several examples of the gestures to be recognized.

To collect the data, a protocol was created specifying the number of repetitions for each gesture and the duration of each associated EMG event. The recorded data was annotated, and the result was the sEMG dataset. This dataset was then used to train and test various machine learning algorithms. This chapter explains all the steps involved in the experiment, which are illustrated in figure 24.

Figure 24 - Steps to achieve a trained gesture recognition machine learning algorithm.

3.7.1. sEMG Gesture Dataset Acquisition

To build the dataset, first a set of five gestures was defined. These gestures were chosen because they are commonly used by humans in their daily lives (figure 25). These are: index extended (figure 25 (A)); index to thumb (figure 25 (B)); closed fist (figure 25 (C)); extended thumb (figure 25 (D)) and spread fingers (figure 25 (E)).

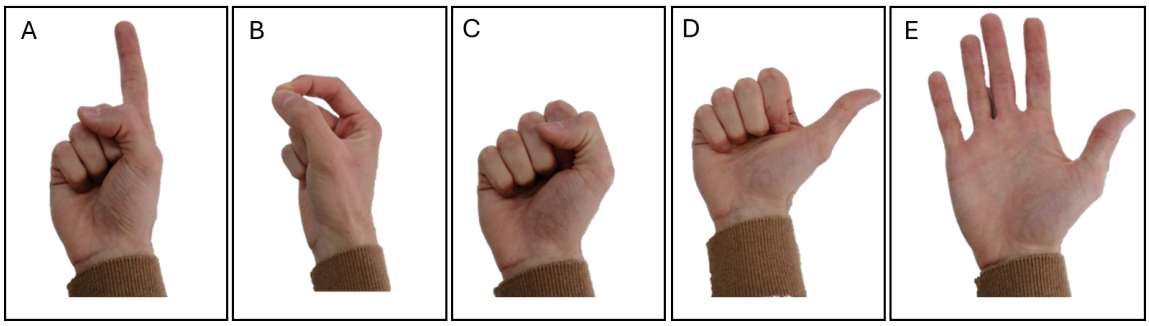

Figure 25 - Dataset gestures (A) index extended (B) index to thumb (C) closed fist (D) extended thumb (E) spread fingers.

The data acquisition was performed using a MYO Armband position on the forearm, as shown in figure 26. The device was aligned with its logo facing upward and the USB port facing downward, as recommend by the Myo Connect, during the calibration phase.

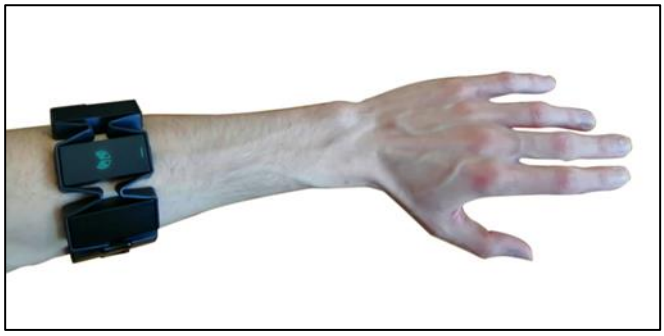

Figure 26 - MYO armband positioning.

The precise position of the MYO armband allows the establishment of correlation between each electrode and the nearby muscles, as shown in the table 3 [30].

Table 3 - Electrode position in the forearm [30]

Eletrode	Muscle
1	*Flexor Digitorum*
2	*Flexor Carpi Ulnaris*
3	*Flexor Digitorum Profundus*
4	*Extensor Carpi Ulnraris*
5	*Extensor Difitorium Cummunis*
6	*Extensor Carpi Radialis*
7	*Brachioradialis*
8	*Pronator Teres*

The MYO armband acquired the sEMG signals using its 8 electrodes in the bracelet, with data transmitted to a computer via Bluetooth. The acquisition used a python algorithm from GitHub [80] and Myo Connect software [81]. Data acquisition was conducted at a sample frequency of 200 Hz. The python software received the sEMG data and stored it in csv files, with filenames referencing the corresponding gesture and session number. For each gesture, five sessions were performed, and each session included 24 motion repetitions alternating with 25 pauses, each lasting 2 seconds. The dimension of the resulting sEMG gesture dataset is presented in table 4.

Table 4 - The sEMG gesture dataset.

Gesture	**Nº Sessions**	**Nº Evts per Session**	**Nº Total Evts**	**Total Duration**
Index extended	5	24	120	240
Index to thumb	5	24	120	240
Closed fist	5	24	120	240
Extended thumb	5	24	120	240
Spread fingers	5	24	120	240

Non-Gesture	**Nº Sessions**	**Nº Evts per Session**	**Nº Total Evts**	**Total Duration**
Relaxing	25	24	600	1200

3.7.2. Segmentation and Annotations

The segmentation and annotation process was unsupervised. The steps of the algorithm applied to segment all the dataset, is presented at the figure 27 summarized into four steps.

In the first step, each session file containing sEMG info from the 8 electrodes, was segmented using an algorithm based on the RMS curve of the electrode. The next step identifies the segmented electrode with the highest Signal Noise Ratio (SNR) of the eight, the master electrode. This is used in the following step to define the threshold values to split between movement and relaxation data. The threshold values are applied to all eight electrodes of the session as division points between movement and relaxation.

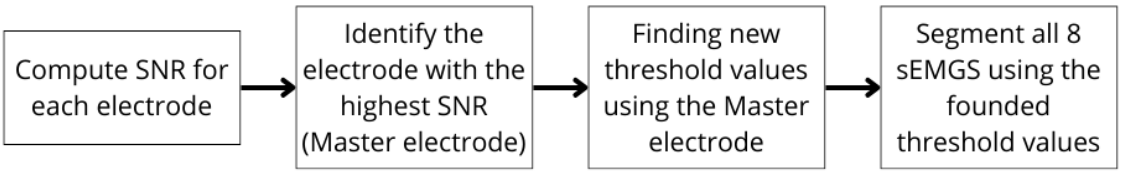

Figure 27 - Flowchart of the session segmentation algorithm.

The segmentation task was performed in MATLAB, where the segmentation algorithm was applied to all gesture's sessions. For each session, the sEMG data was processed by computing the root mean square (RMS) curve for the signals from all 8 electrodes using a sliding window of 100 samples. A predefined empirical threshold was used to compute the SNR for each electrode. All the samples with values greater than or equal to the threshold, were summed to determine the signal energy, while the remaining samples were summed to determine the noise energy. The electrode with the highest SNR, was designated as the Master Electrode, as it defined the segmentation marks for the other electrodes in the csv file. The Master Electrode typically correspond to the one closest to the muscles activated during the movement.

The segmentation of the Master Electrode is performed in two steps. First step aims to find the optimal threshold value. It is an iterative process where multiple RMS-based segmentation are performed. The threshold value is varied from zero to half of the maximum RMS value. The threshold value that produces a segmentation result with a number of EMG events closest to 25 is selected as the optimal threshold. The second and the last step used the selected threshold to perform the final segmentation on the Master Electrode. The resultant segmentation marks are then applied to the signals from all the remaining electrodes. At the end of this process, the target movement and corresponding segmentation marks are recorded in a csv file.

3.7.3. Feature Extraction

To train and test the classifier, a feature vector representing each sample gesture was computed. The data was first normalized, and subsequently, four features were extracted from each gesture sample. The features are: Root Mean Square (RMS), eq 5; Variance (VAR), eq 6; Standard Deviation (STD), eq 7; and Power Spectral Density (PSD), eq 8.

$$RMS = \sqrt{\frac{1}{n}.\sum_i^n {x_i}^2} \quad \text{(eq 5)} \qquad VAR = \frac{1}{n-1}.\sum_i^n |x_i - \bar{x}|^2 \quad \text{(eq 6)}$$

$$STD = \sqrt{\frac{1}{n-1}.\sum_i^n |x_i - \bar{x}|^2} \quad \text{(eq 7)} \qquad PSD = \frac{1}{n}.\sum_i^n |X(w_i)|^2 \quad \text{(eq 8)}$$

The features selected are commonly used in literature, as referenced in studies by Morales et al. (2017) and in Amin et al. (2021) [30], [72]. These features were computed for all the gestures samples and the resulting data was saved in a *csv* file.

3.7.4. Data Classification

The dataset was divided into two subsets: the training set comprising 75% of the available data for each gesture and a test set containing the remaining 25%. The classification experiment involved training a binary decision tree alongside other types of classifiers such as support vector machine (SVM) and neural networks (NN). The hyperparameter used were the ones already predefined by Orange. The SVM used a regularization parameter of 1; regression loss epsilon (ε) of 0,1; kernel of Radial Basis Function. The NN used 100 neurons in hidden layer, Relu activation; L-BFGS-B Solver; regularization (*α*) of 0,002; and a maximum of 200 iterations. This approach is consistent with the methodologies reported in Morales et al. (2017) and Amin et al. (2021) [30], [72]. In Morales el al. work a feed forward neural network was used with 10 hidden layers and an SVM model which the hyperparameter are not mentioned. In Amin work and Artificial Neural network as a SVM and their hyperparameters are not mentioned.

Chapter 4 - Results and Discussion

In this chapter all the results obtain in the work are shown. A discussion of these results will be provided, explaining them in detail and outlining the reasons behind their achievement.

4.1. Desing and 3D printing

In this chapter the results of initial sketches, CAD components are shown and discussed, explain their feature and functionalities.

4.1.1. Initial Sketches Results

The sketch of the skeleton of the hand is represented on figure 28 (A). In figure 28 (B) it's possible to observe the finger extension and in figure 28 (C) the flexion.

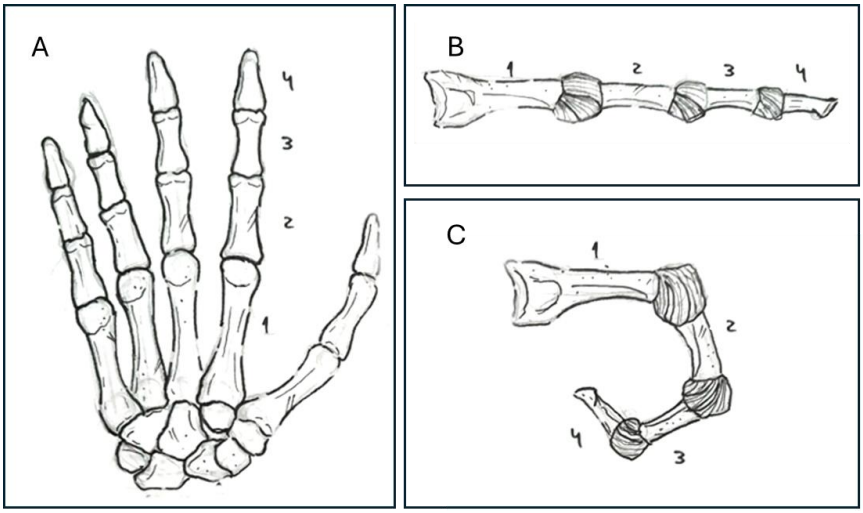

Figure 28 . Sketch of the skeleton of the hand

Three different ways to activate the fingers were considered, these are represented on figure 29. Highlighted in green is represented the movement of the string and in red the closing of the fingers. All three are based on a string attached to a phalange and to a motor, this force is counterbalance by rubber bands between each finger. The first one (figure 29 (A)) it's the simplest of the group, only requires one servo that pulls the a string attached to the distal phalange, the second (figure 29 (B)) each phalange is attach to a string allowing each one to move independently, and the third one (figure 29 (C)) uses a lever mechanism that by only

pulling the proximal phalange and the rest of the finger will close by itself. The second idea was discarded because it would require three motors per finger, this quantity of motors is not reliable due to excess of power, and space that it would occupy. The next phase of the work started to be done with the first and third sketch as foundations, these two systems were named, Model A for the and Model B.

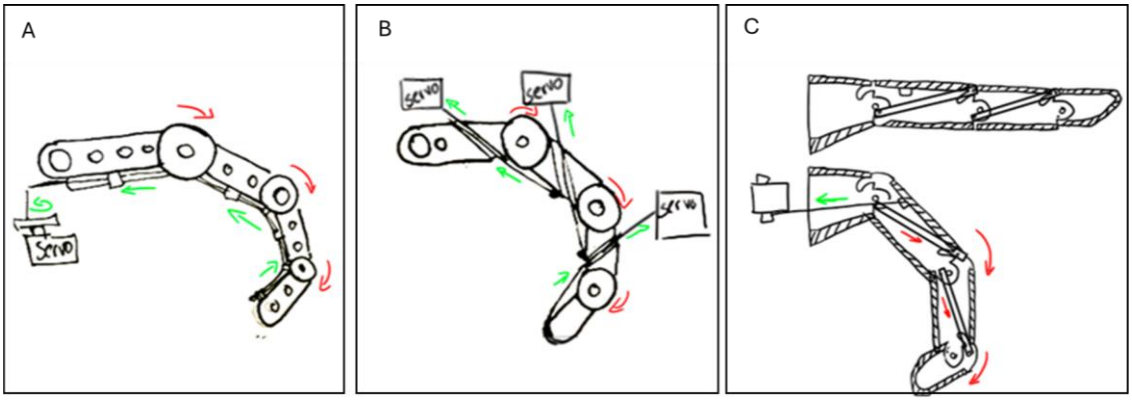

Figure 29 - Sketch of the Action system (A) with one string attached to the distal phalange and to a single servo motor called Model A (B) with three strings attached to each phalange and to each servo independently (C) with lever mechanism using a string attached to the proximal called Model B.

First the joints being designed were for model A (figure 30 (A)). Consisting in two semi spherical pieces that fit together, allowing a revolving motion with an amplitude of 90-degree. Between the two pieces is accommodate a torsion spring to allow the joint to return the original position. The system will be secure by a screw that passes through the hollow spaces inside the parts and the spring, a nut in the opposite way keeps everything together (figure 30 (a1)). The top view can be observed in figure 30 (a2) and the side view on figure 30 (a3). In the other design, specific of Model B, each part will be kept in place by pins that fix the lever inside the finger, this sketch is represented on figure 30 (B) where (b1) shows the top view and (b2) a side view with a cut. These two designs will be repeated for the flexion and extension of the four fingers, and the only thing that will change is the size in phalanges.

For the thumb's adduction and abduction, a joint that works as a hinge powered by the incorporation of a servo inside the hand was designed, as shown in figure 30 (C). In this figure it's also possible to see the passage of the string represent by a dotted line. The rest of the phalanges are articulated in the same way as the other fingers, the type of the model used will depend on the test results.

Relative the hand itself, this part needs to store the thumb's servo, has a spot to fix the fingers, and has a hollow body to allow the passage of strings and the wires from the sensors. The idea was to create a modular system between the main fingers and the hand. Two different sketches were created, as shown in figure 30 (D), one that fits the model A (figure 30 (d1)) and other for model B (figure 30 (d2)).

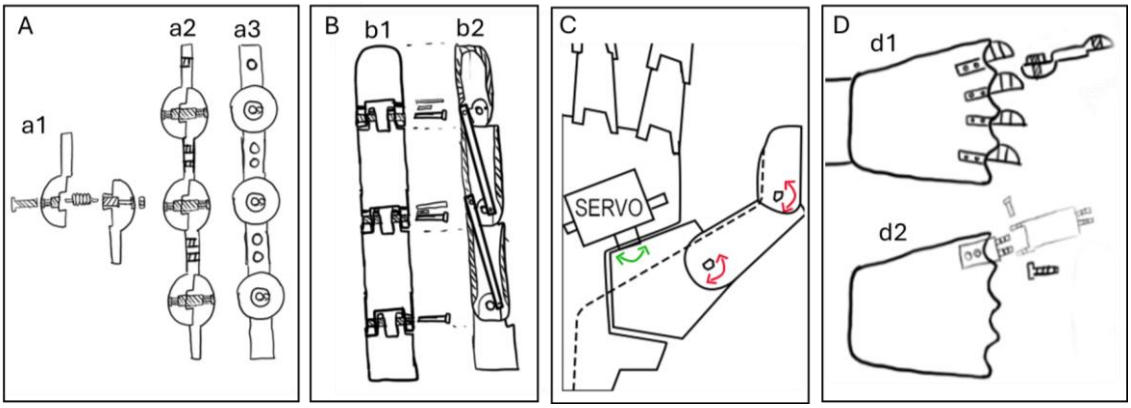

Figure 30 - Joint design of (A) Model A (a1) joint components (a2) top view cut (a3) side view; (B) Model B (b1) top view (b2) side view cut (C) Thumb with hand; (D) Fingers with the hand (d1) for model A (d2) for model B.

The fingertips are responsible to accommodate one temperature sensor, one pressure sensor and to anchor the extremity of the string. The incorporation of these sensors will help the user to interact with the environment by giving the information about the temperature of the object that is holding and understand how much force is being applied by the prosthetic hand. The idea for this design is based on the work of Lanigan et al (2017) [29] where a system in the distal phalanges was created to receive the sensors. This can be seen in figure 31 (A), this component contains two spots, one in the base for the pressure sensor and another in the upper part for the temperature sensor. Highlighted in blue in figure 31 (B) and (C) is represented the pressure sensor. When pressure is applied the structure bends compressing the sensor inside. The temperature sensor will be placed above the pressure chamber, the spot designed to exact measurements and is highlighted in red in figure 31 (B) and (C).

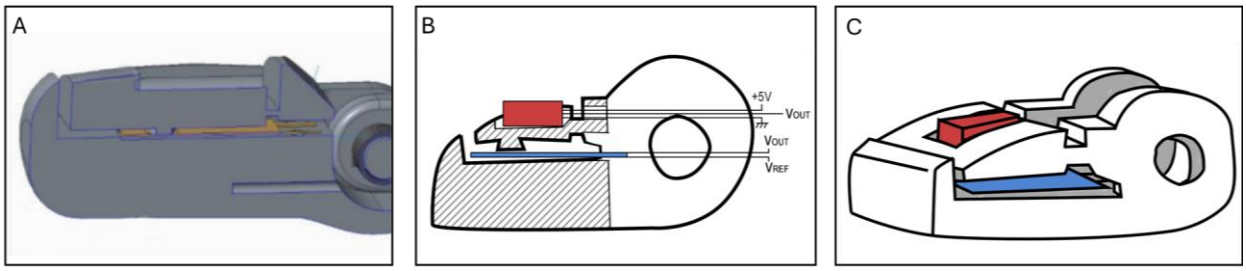

Figure 31 - Fingertip (A) from Lanigan and Tedesse work [29] *(B) sketch side view cutted (C) sketch three plane*

4.1.2. Computer-Aided Design Results

This chapter focuses on the CAD results. Is divided into five sections that focus on different parts of the model, namely the fingers, hand and thumb, wrist, electronic case and model support. All the features and purpose of these components in final model represented in figure 32 is explained in this chapter.

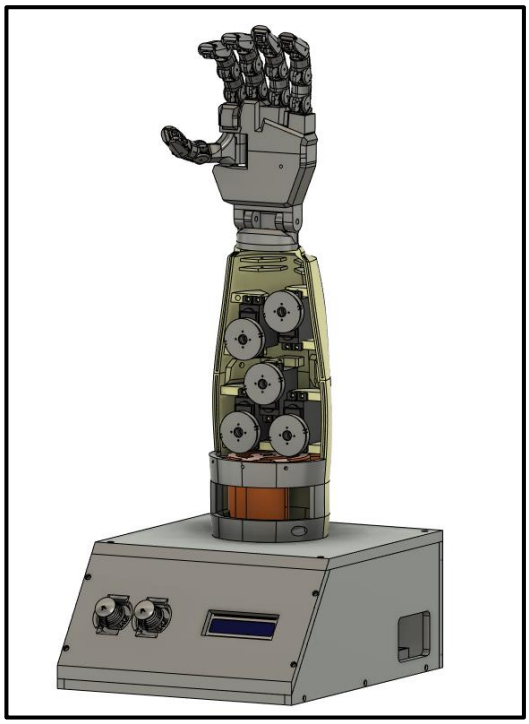

Figure 32 - Final model full assembly.

Finger Design Results

The Model A is shown on figure 33 and is composed by two parts the skeleton and the covers. In figure 33 (B) it's possible to see the model disassembled and highlighted in red the covers and in grey the skeleton.

The covers are responsible to create a more human like finger and could be printed with a soft material as *thermoplastic polyurethane* (TPU), with this the hand can achieve a better grip when holding objects. The skeleton is responsible for structural support, is in this part that the articulation points are contain alongside with the string passages. These were created inside the phalange interlocking the string with the finger. In figure 33 (D) an internal view of the passage is shown and in figure 33 (C) an external view of the system can be observed.

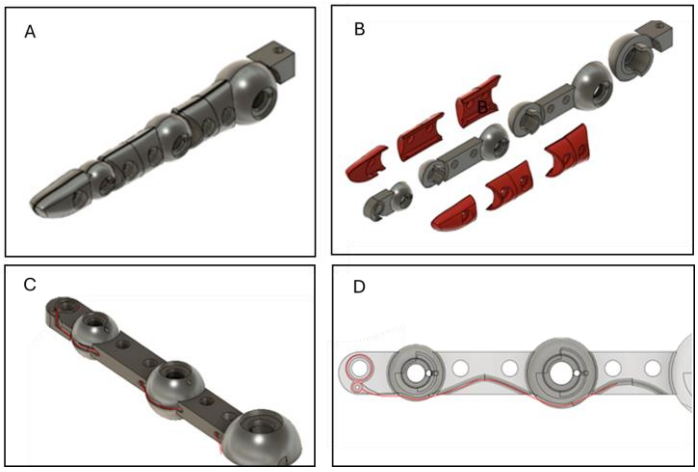

Figure 33 – Model A CAD (A) three plane view (B) components (C) string path (external view) (B) string path (internal view).

The model B is composed by two parts: the phalanges and the levers. The model can be observed in figure 34 (A). Is possible to observe how the different components fit together in figure 34 (B). Each phalanx was divided in two parts, left and right, to facilitate the assemble process of the lever inside. After the design the sharper corners were smoothed to achieve the shape of a real finger, and artificial joints were created in the software. These points of articulation allow to see how the mechanism of levers worked. Figure 34 (C) to (E) shows a progressive movement of the finger only by pulling down on the first phalange.

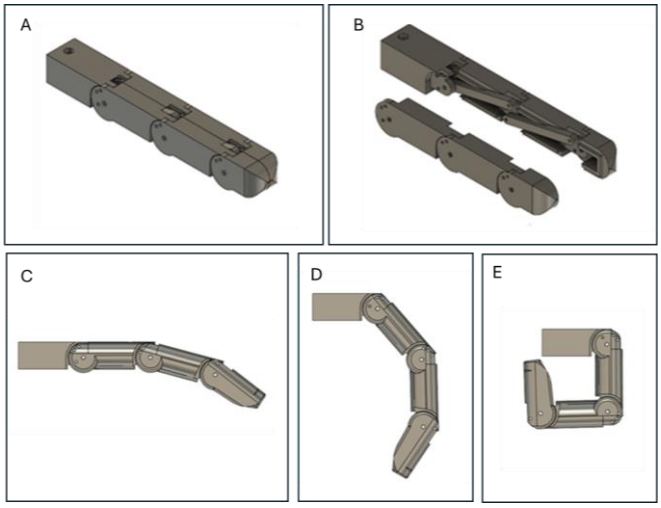

Figure 34 - Model B CAD (A) three plane view (B) components (C) in total extension (B) in semi-flexion (C) in full flexion.

Regarding model C, this combines characteristic from the two previous models, carrying the external design from the model B and the actuation system form the model A. This can be observed in figure 35 (A). Two extra features were added to allow a proper function of the model, a system to keep the rubber bands in place and a way to accommodate the artificial

tendons. Two hooks in each phalange were designed for the rubber bands, in figure 35 (B) is possible to observe the placement of the rubber bands in blue, green and yellow and to understand how they interlock between phalanges. The second difference is represented in figure 35 (C), the string is highlighted in red and is fixed to the distal phalange and passes through the other two. As a result of the structure being based on model B, the interior space for the lever was left empty. This space was later amplified to accommodate the sensor's cables.

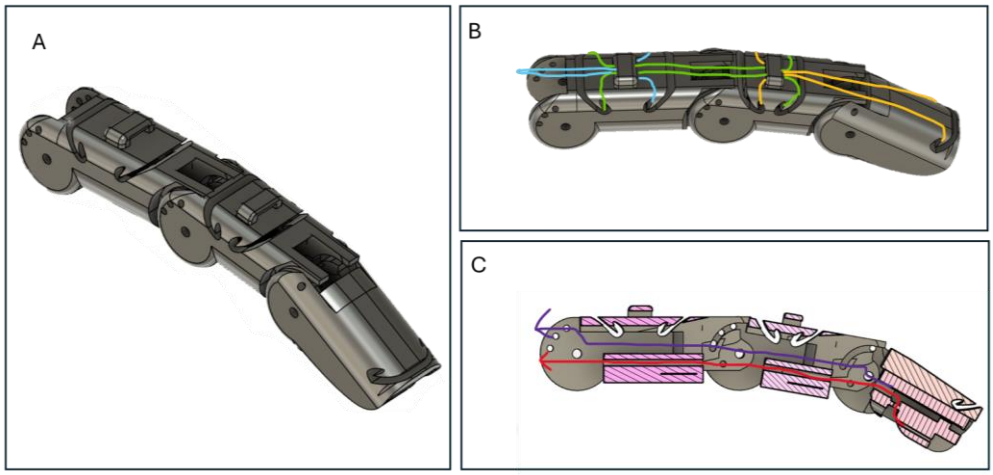

Figure 35 – CAD of Model C (A) three plane view (B) placement of the rubber bands (C) side view with cut in purple wire passage and in red string position.

Hand and Thumb Design

The hand was created with intent to accommodate different features that allow for the proper functioning of all system, the general view of the model is shown in figure 36 (A). Tubular paths were incorporated for the passage of the artificial tendons. These can be seen in figure 36 (B) highlighted in red and green, where the green line represents the string coming from the thumb. It was necessary to allow the passage of cables for the exchange of information between the microcontroller and the sensors, for that rectangular holes in the front part of the hand were designed. These can be observed highlighted in orange on figure 36 (C) and (D). T-shaped protrusion was created in the front upper part of the hand to secure the rubber bands, as can be seen in figure 36 (D) highlighted in bright green.

A cover was designed to enclose all the internal features of this component. It will snap onto the upper part of the hand and secure in place by two screws. A top view of this piece is shown on figure 36 (E), while in figure 36 (D) the bottom view is shown.

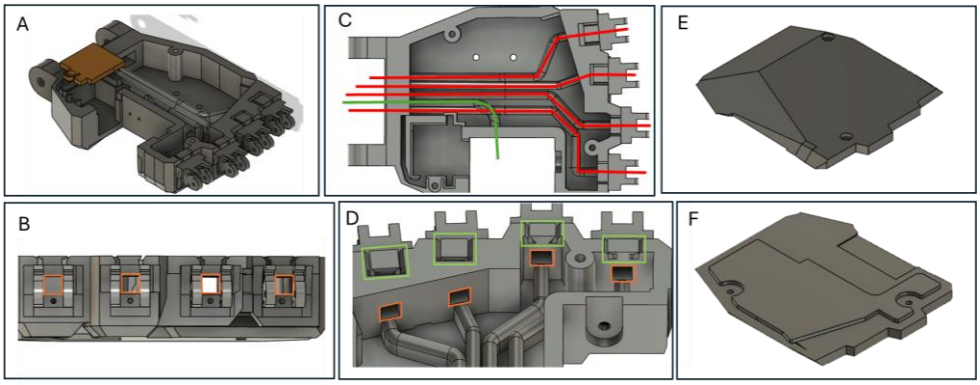

Figure 36- CAD model of the hand (A) three plane view (B) top view (C) front view (D) back view (E) hand cover top view (B) hand cover down view.

The thumb is composed of two phalanges and a metacarpal bone, their assembly can be observed in figure 37 (A). The placement of the rubber bands is illustrated in figure 37 (B) in green and yellow. The servo responsible for actuating the system is accommodated in the hand, as shown in figure 37 (C) and fixed to base of the metacarpal. Highlighted in red on figure 37 (B) it is possible to see where the servo head will fit and held in place by a screw. The thumb's base has a cylindrical protrusion highlighted in light blue in figure 37 (A), that fits inside a groove on the hand, the joint is shown in figure 37 (C) 37 (D) highlighted in light blue. The base is also responsible for mediating the passage of the artificial tendon that comes from the distal phalange, represented in orange on figure 37 (D).

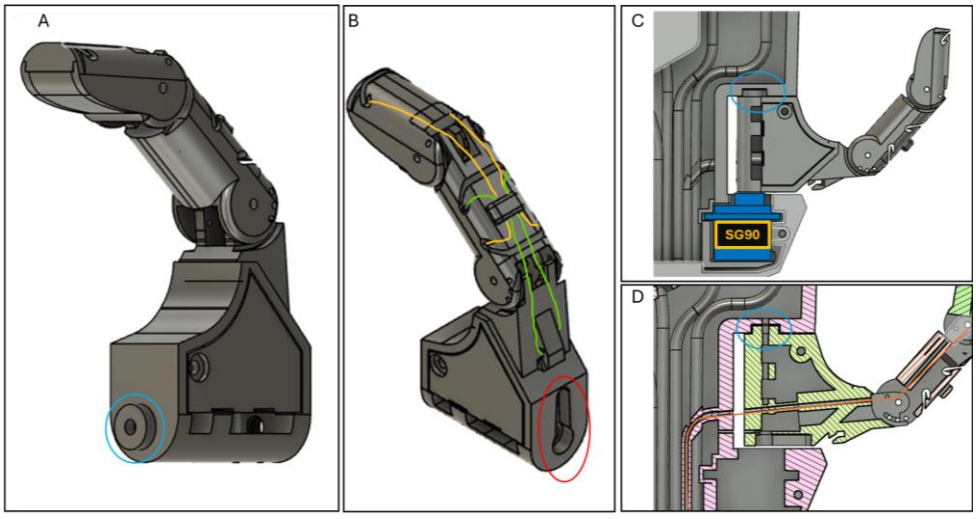

Figure 37 - Thumb CAD Model (A) general view (B) back view with rubber bands (C) thumb-hand joint with servo SG90 (D) thumb-hand view inside view.

Fingertips Design

The fingertips are composed by two parts, the base and the cover. The base (figure 38 (A)) is responsible to slide inside the distal phalange and have a cavity for the pressure sensor to stay in place. The cover (figure 38 (B)) sits above the base and has the function of secure the temperature sensor in the cavity on the top. The component contains a protrusion in the lower part to concentrate the pressure on the sensor when the finger touches an object. The full assembly can be observed in figure 38 (D).

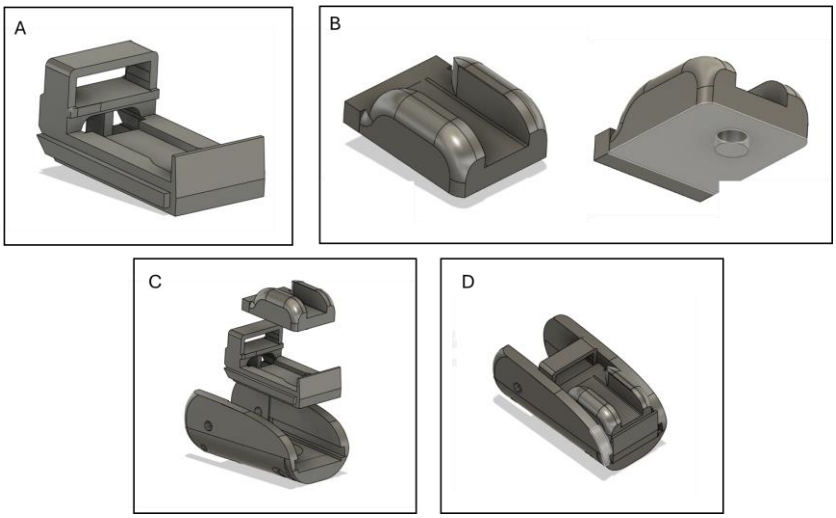

Figure 38 - Fingertips (A) base component (B) cover component (C) all components (D) assembly.

Wrist

This component is very straight forward, with all the views represented in figure 39, it's composed only by one part, as its real-life version mediates the connection between hand and forearm. It connected in three points, two with the hand allowing flexion and extension motion highlighted in blue in figure 39 (A) and one with the forearm that is fix in place by six screws outlined in blue in figure 39 (B). This part also mediates the passage of the strings between the hand and the forearm. This is highlighted in red in figure 39 (B) and (C).

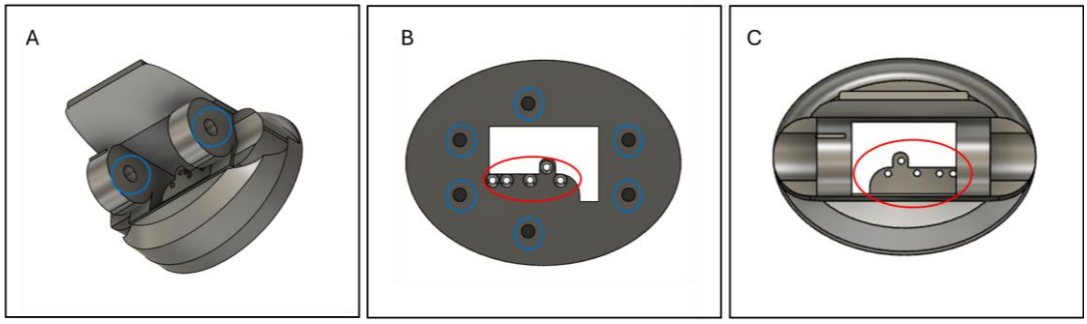

Figure 39 - Wrist CAD Model (A) three plane view (B) back view (C) front view.

Forearm

This component is responsible for securing the servo motors and the rotation mechanism of the forearm. It is divided into three systems, forearm structure (figure 40 (F) in light yellow), the string separator (figure 40 (F) in green), and the rotation mechanism (figure 40 (F) in orange).

This structure contains the connection to the wrist, highlighted in red on figure 40 (A), and a connection to the base, outlined in blue on figure 40 (D). This section accommodates the MG995. Internal structures were created to secure the motors, as highlighted in red on figure 28 (B). The main structure is divided into four parts, that are connected with four sections that overlap the adjacent part and contain two holes for screws. These are highlighted in green on figure 28 (C) and (E). In front of the servos, a piece was added to separates and guide the strings their corresponded motor. This part can be observed in figure 40 (G), while figure 40 (H) shows how this part fits in the forearm.

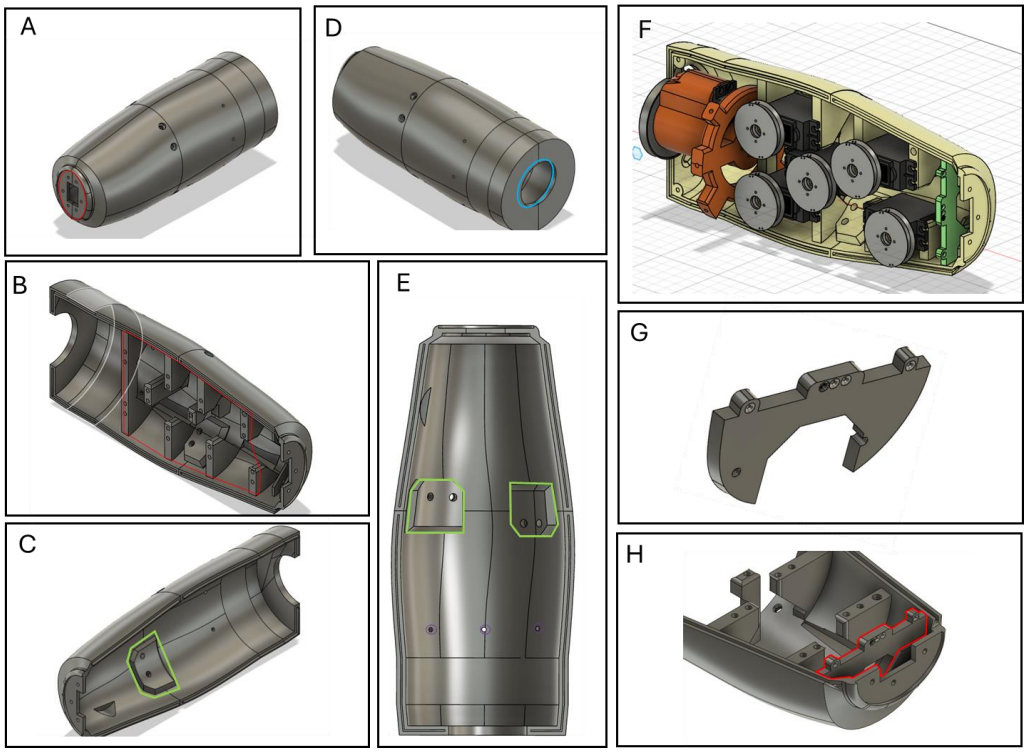

Figure 40 - Forearm structure CAD model (A) closed system front view (B) upper part (C) lower part (D) close system back view (E) interior cover connectors (F) full assembly (G) string separator (H) string separate in place.

4.1.3. Electronic Case and Model support

To support and secure the model during testing, shelter all the electronic components including the breadboards and Arduinos, a box was designed in CAD. The model is shown in figure 41. The box is composed of eight panels, designed to be printed on a small to medium size printers. These will be secured in place by screws. The top panel contains four screw holes to the forearm and other 2 semicircular holes to allow the passage on cables (figure 41 (A)). The front panel includes three spots to fix a 16x2 I2C LCD and two joysticks to control the hand movements (figure 41 (A)). The left panel has a rectangular opening to pass power supply cables, if necessary, (figure 41 (A)). In the interior three slots were created to fit the three breadboards and two others to fit the two Arduinos (figure 41 (B)).

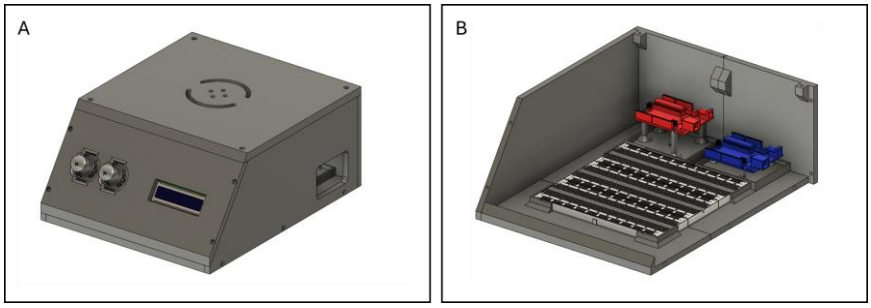

Figure 41 - Electronic case and Model Support (A) outside view (B) interior view.

4.2. Actuation Tests Results

This section approaches all the results obtain in the tests involving the finger models and servos systems. With these tests the model with better performance will be establish, as well as the servo system that will be used in the final prototype. Capability of motor to close the fingers without struggling and the efficiency of the finger to return to the resting position will be evaluated. The figures that will show the results are divided into three sections, (A) the moment before servo actuation, (B) the moment during servo actuation and (C) the moment after servo actuation.

4.2.1. Auxiliar Components Results

Firstly, a modular base was designed, with the ability to expand using similar parts. Its body is composed of matrix of sixty-three holes with three millimetres in diameter allowing to fix other modules on top. This component can be observed of figure 42 (A). To fix the fingers

to the base, simples' parts were also created to mediate the connection. These parts are shown in figure 42, for the model A in figure 42 (B), for model B and model C in (C).

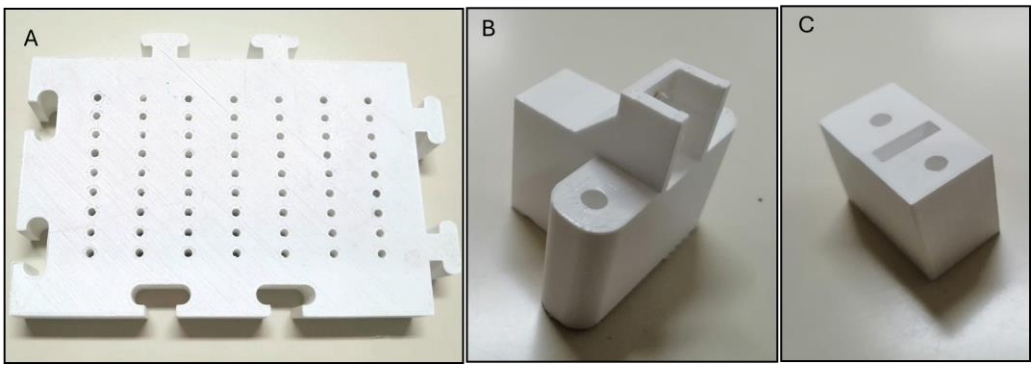

Figure 42 - Support components (A) Modular base (B) Model A connector (C) Model B and C connector.

For the servos three types of modules were created, two for the SG90 and one for the MG995, all these have the objective to rotate a pulley that will pull a string and close a finger.

For the SG90, the first module held only one motor with a pulley attach to its head, this system's parts are represented on figure 43 (A), and the full assembly in figure 43 (B). The second module uses two motors combining their torques into one pulley via a system of three gears from the same ratio, two attached to each servo and one in the pulley. The components of this module are represented in figure 43 (C). To minimize mechanical energy loss, the servo head was encapsulated inside the gear during 3D printing.

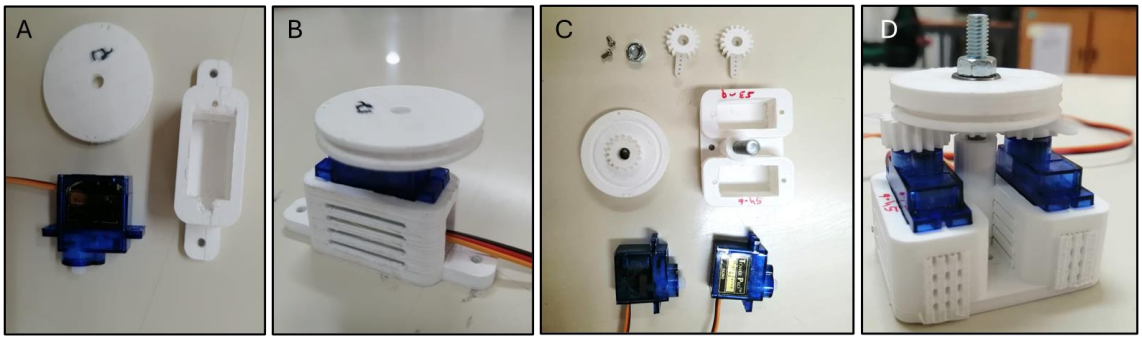

Figure 43 – SG90 system (A) single sg90 system components (B) single sg90 system assembly (C) double sg90 system components (D) double sg90 system assembly.

The module for the MG995 is compose of a case, the motor and a pulley. The full assembly is represented in figure 44 (A). The pulley was built with an encapsulated servo head inside, in the same manner as the gear describe before, these parts are shown on figure 44 (B). Due to the high torque of MG995 it wasn't necessary to create a second system like the SG90 using two motors.

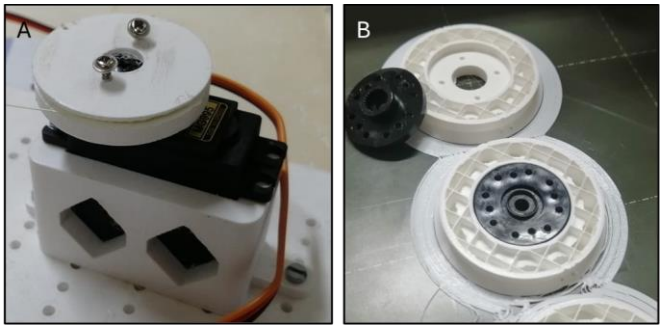

Figure 44 - Single MG995 module (A) full assembly (B) pulleys.

4.2.2. Fingers Actuation Tests Results

Single SG90

For the single SG90 tests, represented on figure 45, it is possible to see that the only model capable of being actuated by the servo system was model C. Model A couldn't close because the force imposed by the internal springs was very high. The power of the servo was insufficient and the friction inside of the joints didn't help the process. Model B has similar problem occurs, where the servo was unable to close the finger, despite the model having low resistance. The problem was that the initial push necessary to activates the lever mechanism could not be delivered by a single SG90 servo motor.

Model C on other hand had the better performance, closing and opening with ease Model C was created in this part of the work, during the tests with the SG90. As said before, it combines the good parts of the models A and B, using the actuation system of A and the frictionless design of the B. With this combination, it was possible to make room for cable passage inside the finger, a problem that A and B have in common.

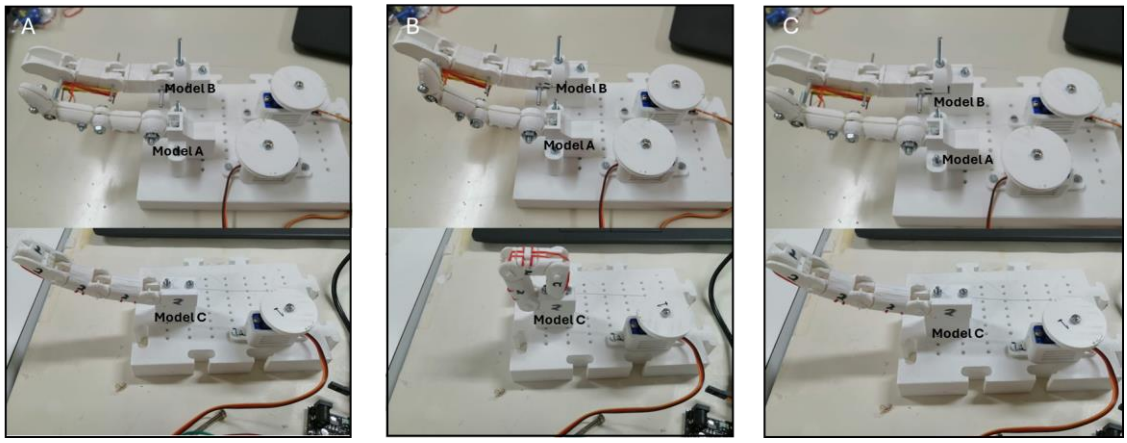

Figure 45 - Single SG90 test (A) before servo actuation (B) during servo actuation (C) after servo actuation.

The results of the double SG90 tests are represented on figure 46, it can be observed that the model A performs much better than in the last test, closing almost totally but even with this increase in performance, didn't work properly. Initially, the actuation was not smooth, with noticeable resistance between the finger and the servos. This behaviour was caused by the springs being too strong. When the servo stops applying force and allow the finger to relax, the high level of friction between the joint parts, prevents the finger of opening. Model B did not show significant improvements compared to the test with a single servo. Despite the low friction between parts, the motors still could not provide the initial push needed to actuate the finger. Model C, as expected, has the best performance, executing the job with efficiency.

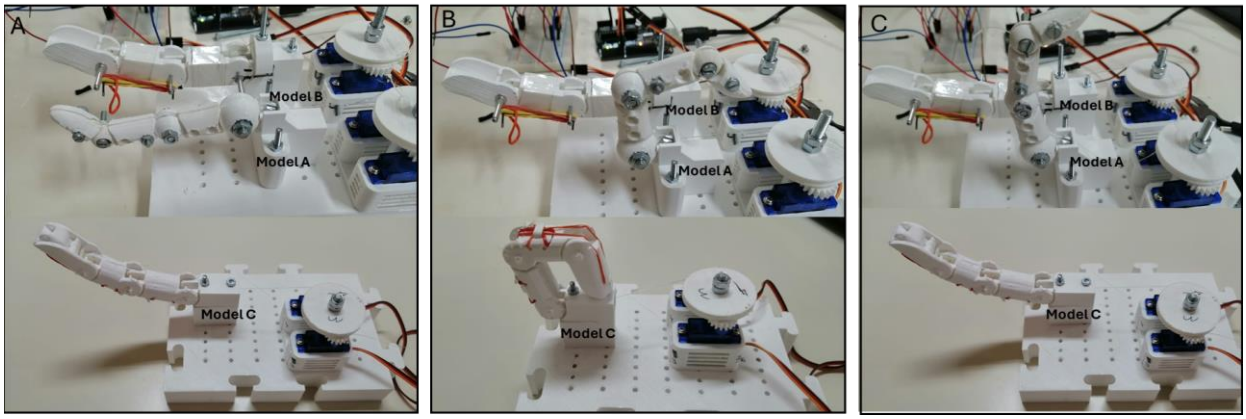

Figure 46 - Double SG90 Test (A) before actuation (B) during actuation (C) after actuation.

The MG995 were the second motor choice. Figure 47 shows the test apparatus with these motors. All models were actuated without difficulty (Figure 47 (B)). However, when the fingers returned to the resting position, Model A failed to do so due to friction between its parts. Similarly, Model B encountered the same issue, but this was caused by the rubber bands jamming between the joints. On the other hand, model C closes totally with ease and returns without difficulty to the resting position.

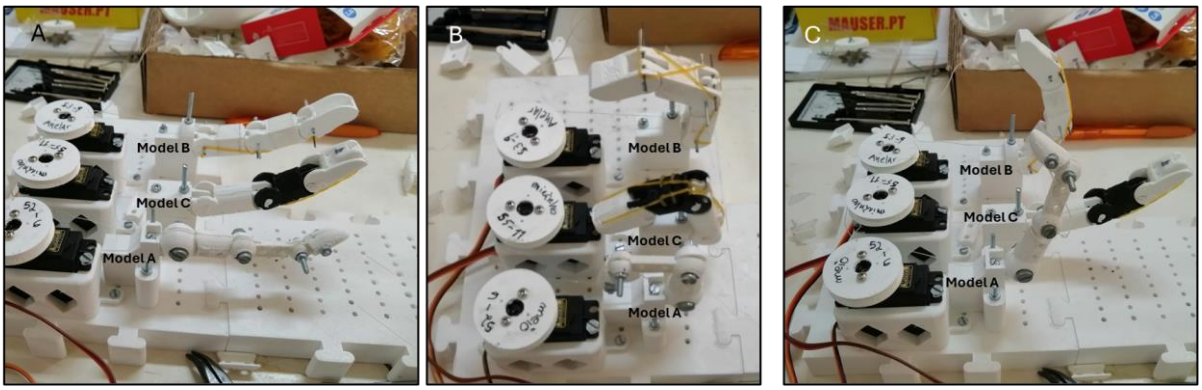

Figure 47 - Single MG995 test (A) model A. B, C before servo actuation (B) model A, B, C during servo actuation (C)model A, B, C after servo actuation.

After this final test its clear that model C is the most efficient and that the MG995s are much superior to the SG90s. Although the SG90 servos were capable of handling Model C, it is better to use the MG995 servos. The MG995 offers better grip, is built with metal gears, is more reliable, and provides higher torque. Additionally, the inclusion of wires for the sensors will increase the resistance within the model, potentially causing issues for the SG90 servos, which are already operating near their failure point. The use of these larger motors is only feasible because this work envisions future development of a full prosthetic arm. With the forearm currently empty, there is sufficient space to accommodate these devices.

Thumb Actuation Test Results

To test the thumb, this part was assembled into the hand, and the SG90 servo motor was initially tested for a 90-degree rotation, shown in figure 48 (B), and after that the flexion and extension were tested as can be seen in figure 48 (C). The SG90 performed without problems because the only force that offers resistance the motor is the weight of the thumb itself, and the friction between the piece has been minimized by the design and by sanding the surfaces. The MG995 in the flexion and extension also showed a good performance, closing and opening the finger without resistance.

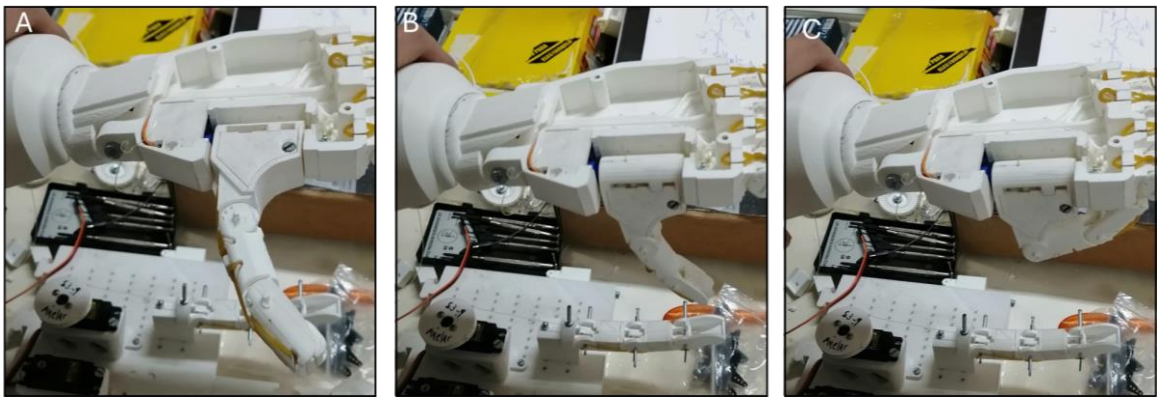

Figure 48 - Thumb (A) in rest (B) abduction/adduction test (C) Flexion/extension tests

4.3. Electronic and Sensory Component Results

The results related to the testing, and performance evaluation of the various electronic components involved in this work are detailed and discussed within this chapter.

The sensory module captures information about the object grabbed by the hand and sends it to the microcontroller after being conditioned. Since the chosen microcontroller platform has a limited number of ADC ports, making it impossible to connect all the temperature and force sensors simultaneously, multiplexers had to be used. The multiplexing module is responsible for routing the sensors data to the control system module. The control system module is composed of two microcontrollers. The first one (microcontroller 1) controls the routing and digitize the pressure sensors data to limit the force applied on a held object. The flexion and extension of the fingers and abduction and adduction of the thumb are also controlled by this board. The second one (microcontroller 2) is responsible for routing and digitize temperature sensor data to give feedback to user about the temperature of held object. This feedback is given via an alarm and a display in the back of the hand. This part also controls the rotation of forearm. The architecture of the system is shown in figure 49.

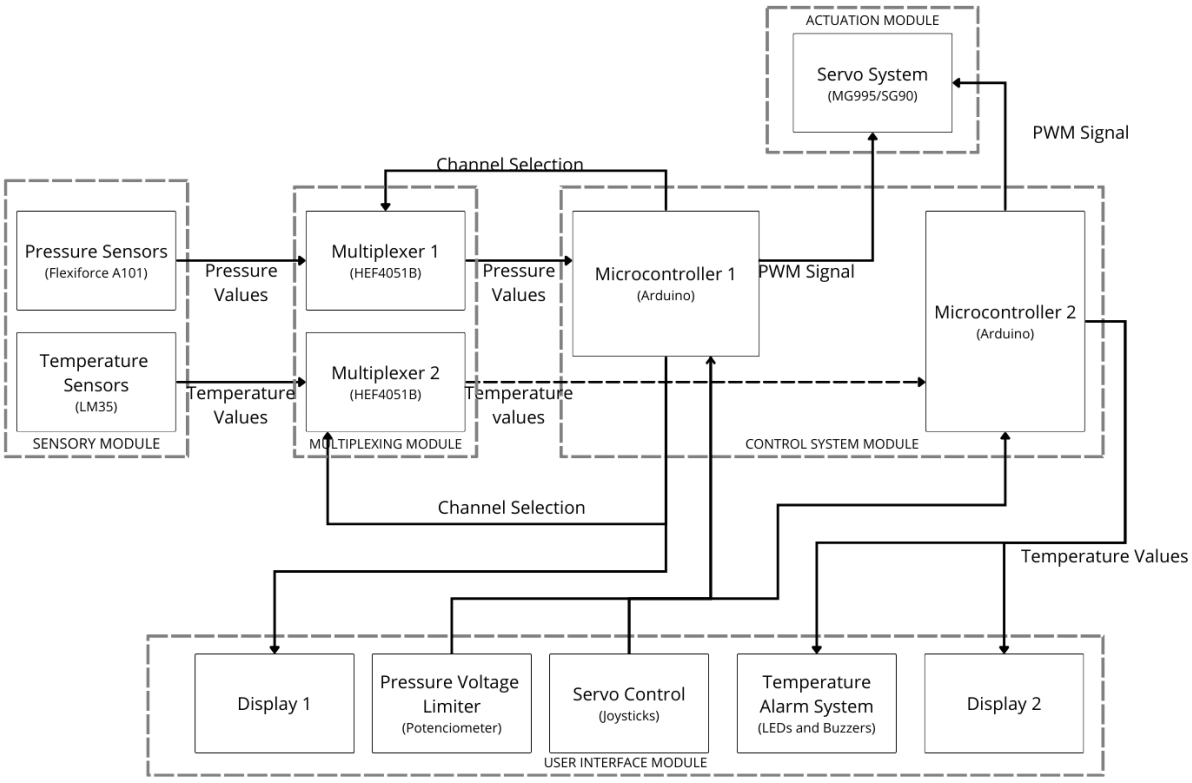

Figure 49 - Blocks diagram of the electronic circuit of the project.

4.3.1. Sensory Module Results

This section shows all the results obtained in the sensory component chapter during calibration and testing of the sensors. It highlights advantaged and limitations of the electronic components during the experiments, providing a clear understanding of the sensors' performance.

Pressure Sensor Calibration Results

For the A101 sensor, the designed loading cell can be observed in figure 50. With the calibration was possible to create a table comparing the changes in applied force with corresponding changes in resistance and conductivity during the calibration process. The loads were applied progressively, and the amplifier voltage values were recorded, as shown in table 5.

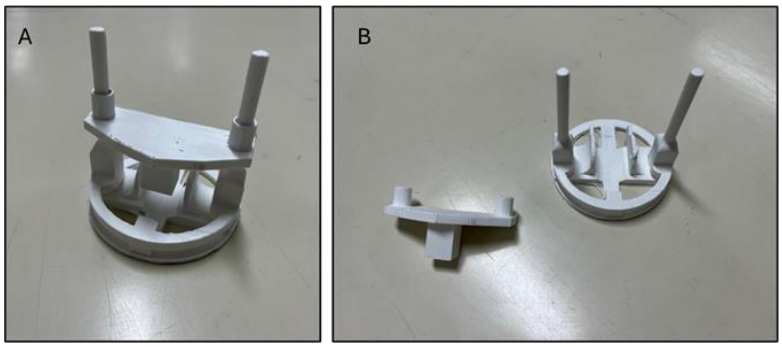

Figure 50 - Loading cell (A) assembly (B) components.

Table 5- Result from calibration of A101

Weight(g)	Voltage(V)	Resistance(KΩ)	Conductivity(1/R)
0	0,05	10000000,0	0,0000001
50	0,1	5000,0	0,0002
150	1,05	476,2	0,0021
200	2,25	222,2	0,0045
300	3,94	126,9	0,00788
350	4,41	113,4	0,00882
450	4,94	101,2	0,00988

The relationship between the voltage and A101 sensor's resistance variation is nonlinear, but is linear with the A101 sensor conductivity. The graph illustrates the variation in resistance and conductivity as a function of applied force are presented in figure 51. Figure 51 (A) represents the values obtained during calibration and figure 51 (B) presents the data provided by the supplier. The sensor´s operational limit is reached at 450g of weight.

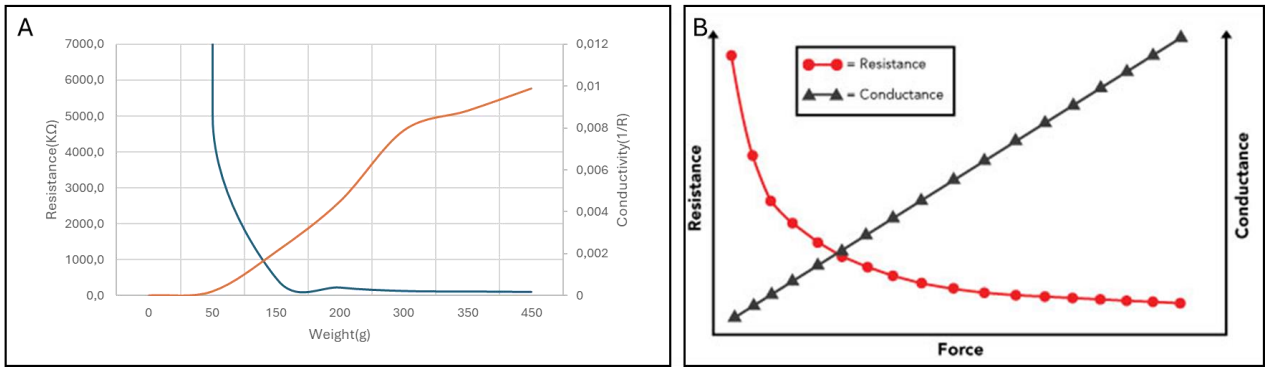

Figure 51 - Results from A101 (A) obtained in the calibration (B) given by the supplier.

Temperature Sensor Calibration Results

The calibration results for the LM35 sensor are presented in Table 6, where the differences between the temperature recorded by the sensor and the thermometer can be observed. A small discrepancy exists between these values, because the sensor is not calibrated well and because to its placement on a prototyping breadboard along with the use of one-meter-long soldered wires, which introduce interference. By knowing these differences, it is possible to compensate or adjust the readings values within the code.

Table 6 - Result from LM35 calibration

Lm35 (ºC)	Thermometer(ºC)	Absolute Error (ºC)	Relative Error (%)
27	27,6	0,6	2,2
27,37	27,7	0,33	1,2
28,35	28,7	0,35	1,2
28,84	29	0,16	0,6
29,33	29,9	0,57	1,9
29,81	30,4	0,59	2,0
30,3	30,7	0,4	1,3
30,79	31	0,21	0,7

The comparison between the encapsulated and non-encapsulated LM35 sensors is shown in figure 52. The graph displays two similar curves, sensor without silicone in blue and encapsulated sensor in orange.

There is a small difference in the initial temperature readings, with the encapsulated sensor starting at 28,8ºC and the non-encapsulated sensor at 27,9ºC. This discrepancy is likely due to a measurement error, as both sensors were at room temperature at the beginning of the test and the thermometer marked 27ºC.

The non-encapsulated sensor shows a faster response time, but also produce less stable readings. The sensor with silicone takes longer to respond to temperature changes, requiring almost 6 minute to reach the temperature recorded by the non-encapsulated sensor. However, it provides more stable readings.

The silicone reduces the sensor responsiveness because the temperature is dispersed throughout the silicone material before reaching the sensor. As a result, the encapsulated sensor is less affected by rapid fluctuations of ambient air temperature.

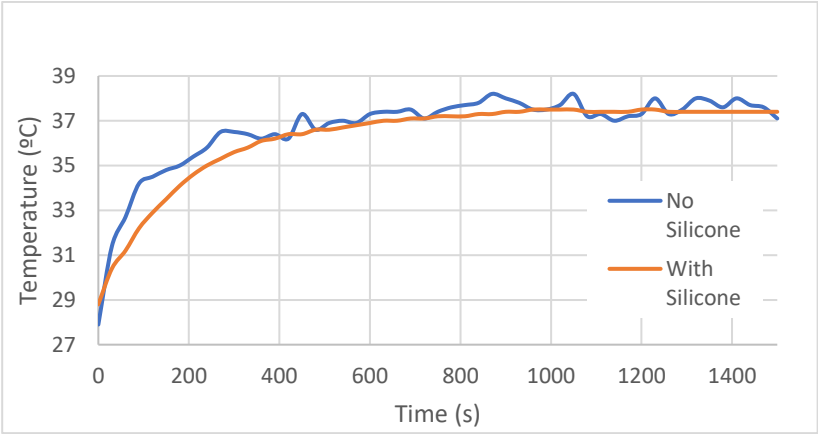

Figure 52 - Comparison between encapsulated and non-encapsulated LM35

Pressure Sensor Testing Results

The results obtained during the testing of the A101 sensor, demonstrated that the system designed to stop the motor when pressure exceeded the desire threshold, performed effectively, stopping the finger from applying further pressure.

Temperature Sensor Testing Results

Regarding the LM35 sensor, the system responded as intended to temperature increase, The LEDs were activated sequentially, from green to red ended up activating the alarm buzzer as intended and displaying the appropriate warning screen on the back of the hand.

4.3.2. Multiplexer Module Results

Functions Test

Table 7 shows the voltage measurements at the Y ports and the Z output of the MUX during the function test. These results reveal a small voltage drop between all the Y and Z ports except for Y6. Although this voltage loss is minor and does not significantly impact the outcomes of this work, it is important to understand as it could affect the sensor values transmitted to the microcontroller if the loss were more substantial.

Table 7 - MUX functionality tests

$Y_{(0-7)}$(A2,A1,A0)	Input(V)	Output-z(V)	Erro absoluto (mV)	Erro relativo (%)
Y_0 (0,0,0)	3,367	3,349	18	0,537
Y_1 (0,0,1)	1,692	1,681	11	0,654
Y_2 (0,1,0)	3,764	3,755	9	0,240
Y_3 (0,1,1)	2,515	2,489	26	1,045
Y_4 (1,0,0)	1,259	1,246	13	1,043
Y_5 (1,0,1)	3,764	3,774	10	0,265
Y_6 (1,1,1)	2,515	2,515	0	0,000
Y_7 (1,1,1)	1,255	1,251	4	0,320

The Multi-Sampling Test

Figure 53 illustrates the behaviour of the voltage values, when the MUX is commuted, between Y0, Y1 and Y3. It's possible to observe that the values change instantaneously as the Y channels are switched. This demonstrates that the readings can be performed at the speed of the Arduinos ADC, ensuring rapid data acquisition.

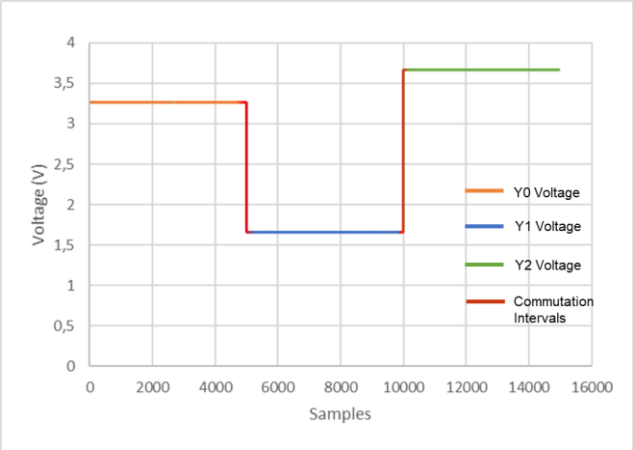

Figure 53 – Multi sampling test results.

4.3.3. Actuator Module Results

After registering the current values for all tests with the MG995 servo, it was possible to verify the maximum and minimum values per test, the results are shown in table 8. Across all tests the motor required a minimum current of 10 mA. This current value is consumed by the servos by only be powered on. Analysing the maximum values it's possible to conclude an increase in current when the wires were added. The wires create more resistance in the finger

what leads to motors making a bigger effort in closing the finger. Is possible to see that test MG5 have the higher current values. The power supply needs to be able to delivery this current values to each servo. The system has six motors of this type making a total of 3,35A only to power the servos.

Table 8 - MG995 current values

Tests	Current Values (A)	
	Min	**max**
MG1	0,01	0,477
MG2	0,01	0,48
MG3	0,01	0,409
MG4	0,01	0,451
MG5	0,01	0,559
MG6	0,01	0,512

4.3.4. Control System Results

All the functions of the system are controlled by the code implemented in both microcontrollers. The logic of this code is illustrated in the flowcharts in figure, where figure 54 (A) is specific of Arduino 1 and figure 54 (B) of Arduino 2.

Arduino 1 gets values from the five A101 by switching the MUX output, also acquires the voltage values from the potentiometer and uses this information to limit the force applied in the object. Additionally, the board receives the input from the joystick button to increase the counter and iterate through the gesture menu. It's important to mention that the servo can be controlled manual by moving the joystick up and down, for flexion/extension and left to right for abduction/adduction movements of when menu six is selected.

Arduino 2 used the same methodology to read all the five LM35 and shows their average value in the display. This value is also used to activate the alarm system if necessary. The other feature that the board is responsible for is to allow for manual control of the servo located in the base of the forearm.

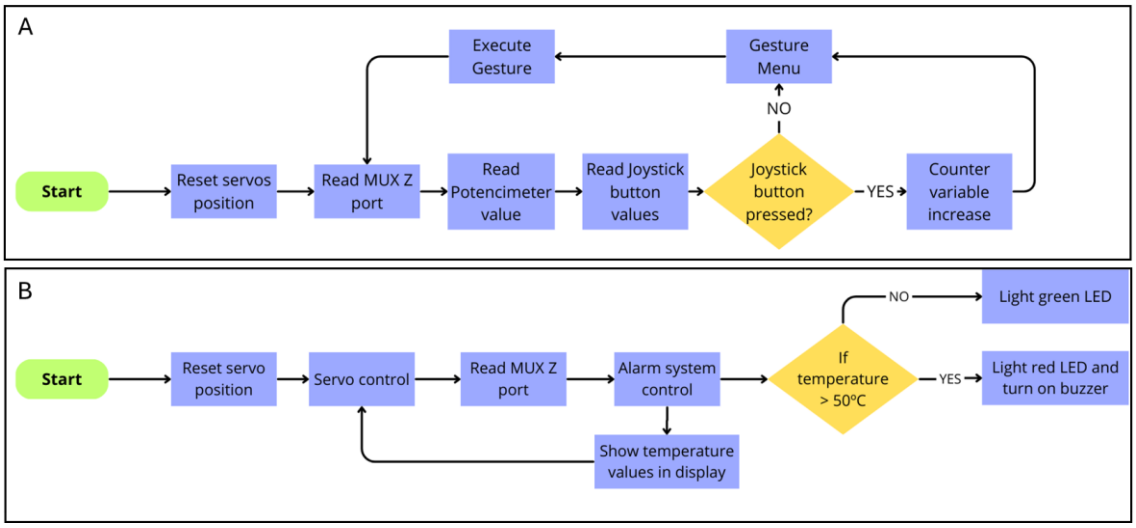

Figure 54 - Code logic flowchart for (A) Arduino 1 (B) Arduino 2.

4.4. Wiring Accommodation and Model Assemble Results

With the model totally assembled it's possible to have a better view of the problems of the system. The wires accrescent more resistance to the opening and closing of finger. This can be solved by changing to a smaller diameter wire. The joint between distal a middle phalange couldn't be articulated properly due to the soldering points of the sensors that enlarge the cables. Was necessary to twist them to pass through the middle phalange. This could cause problems in the soldering points and in the sensors, terminals making them susceptible to break. A solution could be to cut short the sensors terminals to me closer or even inside the fingertip. The phalange joint point should be redesigning to better accommodate the wires. To solve these the phalanges were fused together. By doing so, the stress in the soldering points is removed when opening and closing the fingers. The maximum amplitude of motion achieved between the two phalanges is shown on figure 55 (A) and that was the position where the pieces were fused.

Another issue in this part of the system was that the silicone was applied before attaching the strings to the fingertips. To address this issue, it was necessary to manually create a hole in each fingertip to attach the string. This adjustment is shown in Figure 55 (B), highlighted in red.

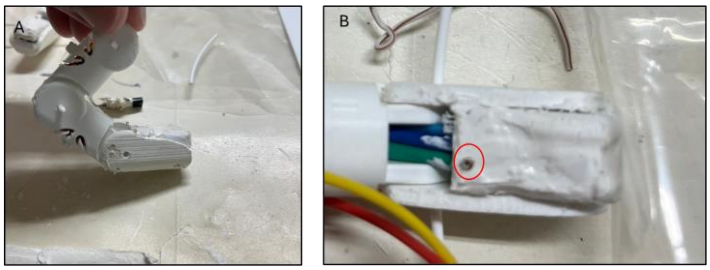

Figure 55 – Problem in the assemble model (A) with distal and middle phalange (B) with wiring passage and string attachment.

Regarding the full assembled model this is represented in figure 56. Was possible to observe some problems too. The finger actuation became less smooth with the addition of wiring and sensors, leading to greater work by the servos. The rubber bands needed to be readjusted to ensure that the finger could properly return to its resting position. The system in place, with string as artificial tendon, works but is not efficient. A lot of energy loss occurs due to the friction between the string and the model components. This configuration is very susceptible to string unwinding and string break. The attachment points, although not optimally designed, serve their purpose. However, they remain a weak point in the model. During testing, the string disconnected from the fingertips, causing the end of the wire to recede into the hand. To fix this it was necessary to open the system. This allowed to conclude that the model is very complicated to work with, the components in the forearm needed to be rearranged to allow for easier maintenance without having to remove many parts.

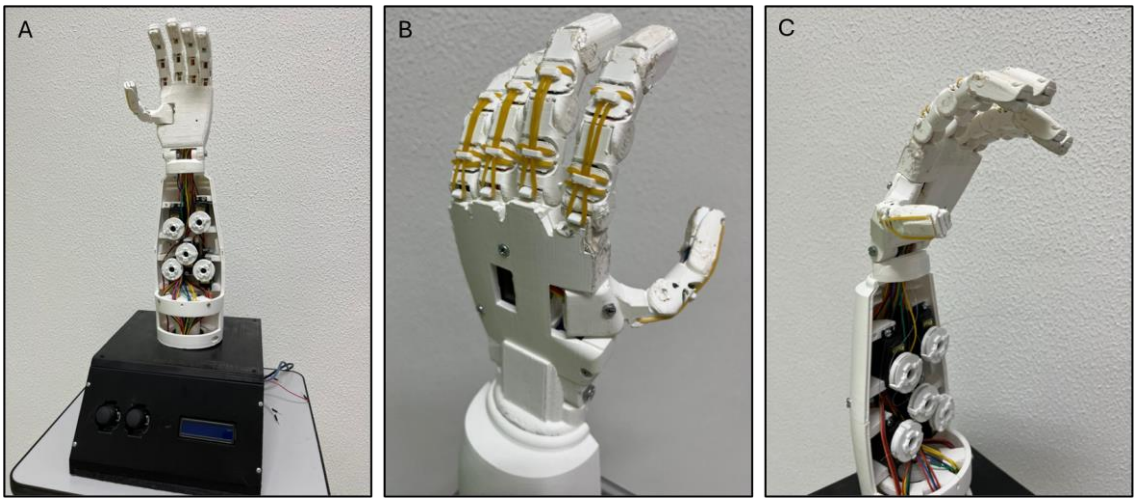

Figure 56 - Assembled model (A) front view (B) of the hand back view (C) side view.

The model was able to execute all the preprogrammed gestures as can be observed in figure 57, but the code needs to be refined. When switching between gesture process occurs to rapidly and this needs to be a slower process to give time to the fingers to change position

without blocking each other. A solution for this could be the addition of a reset position between gesture. Position 2 was the hardest to execute due to the high precision required, which the actuation system in place could not deliver.

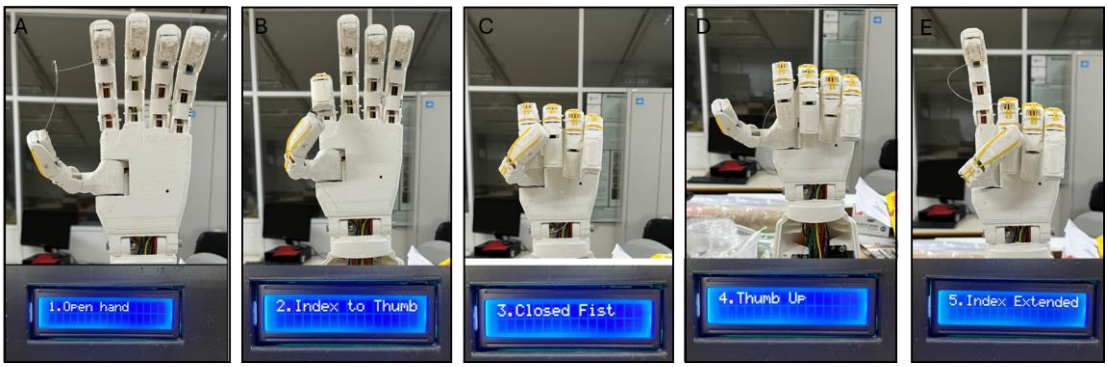

Figure 57 - Preprogramed gesture (A) open hand (B) index to thumb (C) closed fist (D) index extended (E) thumb up.

When holding objects the model was capable of hold all the selected ones, as shown figure 58. Figure 58 (B) shows similar results from the work of Lanigan et al (2017). The model struggles when holding the larger objects (hammer and drill). In the case of the hammer, the model lacks adhesion points and these should be implemented by creating silicone pads in the hand. The drill was just too heavy for the SG90, that holds the thumb, and was almost not capable to counterbalance the force impose by the drill. This can be solved by swopping the SG90 servo for a stronger one like MG90 servo, that has more torque and metal gears.

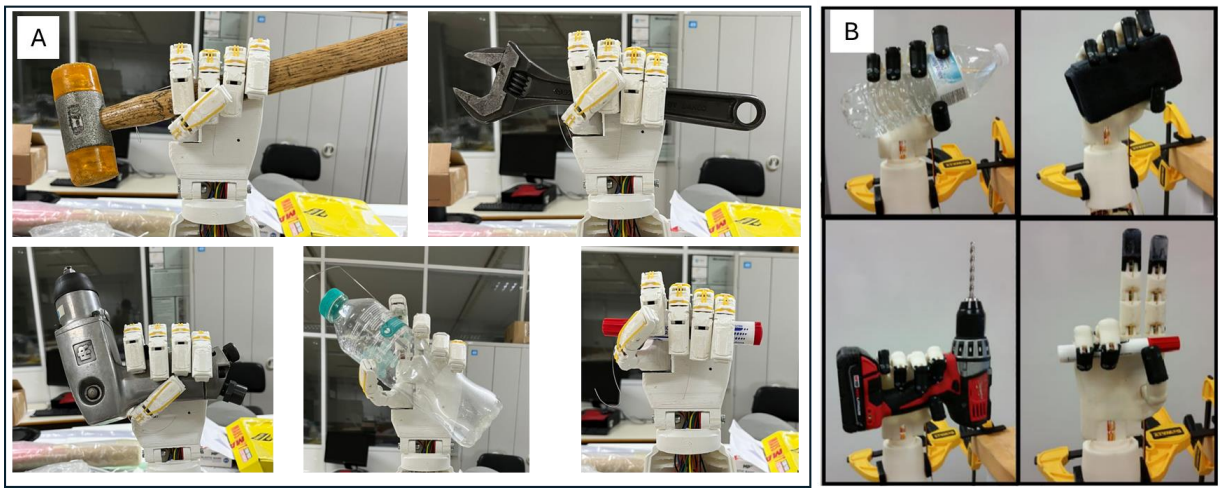

Figure 58 - Held objects test result (A) form this work (B) from the work of Lanigan et al.(2017)

4.5. Gesture Recognition Results

This section presents and discuss the results obtained from the Gesture Recognition experiments using several classifiers. The experiments were performed using Orange program, an open-source toolkit for data visualization, machine learning and data mining.

4.5.1. Data classification Results

The first experiment was done using a binary tree model, resulting in the tree structure shown in figure 59 (A). A decision tree is limited in its ability to capture complex, non-linear relationships in data, where a neural network or support vector machines outperforms in modelling such scenarios due to its layered architecture and capacity for feature abstraction, However, a decision tree provides the advantage of clearly revealing the importance of the criteria used in the decision-making process.

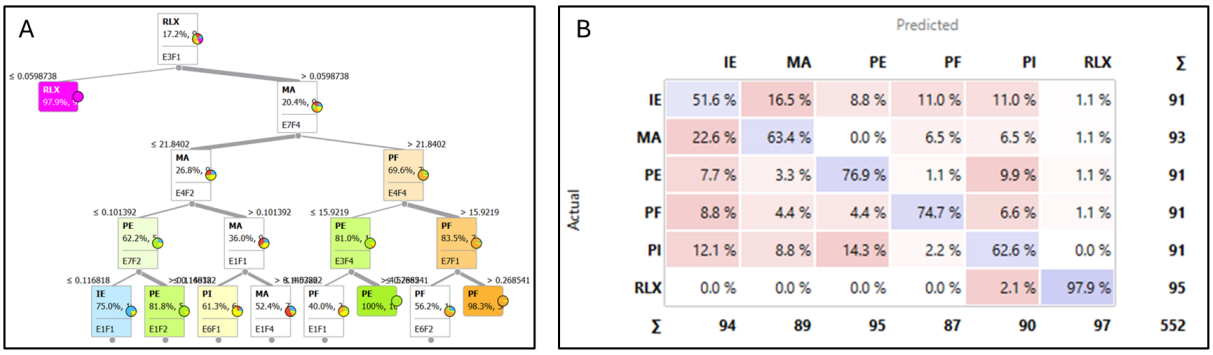

Figure 59 – Decision tree (A) flowchart results (5 depth levels) (B) confusion matrix (IE; MA; PE; PF ;PI ;RLX).

As anticipated, the linear approach using a decision tree reveals several limitations. The IE gesture classification is 51,6%, which is close to a random classification. The PI gesture is poorly modelled, as it appears to share features with IE, MA, PE and even RLX. There is a confusion between RLX and PI, which suggests segmentation issues. This means that both events may contain overlapping from adjacent segments. When observing the decision tree is possible to correlate the electrodes with the gestures. IE is correlated with electrode 1 have an outcome of 75%. MA correlates with multiple electrodes, such as electrodes 1, 4, and 7. PE is associated with the electrode 1, 3 and 7. PF is correlated with the electrodes 4, 6 and 7. PI is related with electrode 6. A further iteration was performed using a non-linear decision approach, based on SVM and NN classifiers, with the results presented in table 9.

Table 9 - Gesture recognition experiments result

Model	AUC	CA	F1	Prec	Recall	MCC
Decision Tree	0,870	0,780	0,775	0,780	0,7809	0,739
SVM	0,981	0,874	0,865	0,888	0,874	0,853
NN	0,993	0,912	0,910	0,912	0,912	0,895

The best result was achieved using a Neural Network classifier with 91,2% accuracy and a SVM obtain 87,4% accuracy. In the work of Amin et al. (2021) was obtain an average accuracy of 96,7% for NN and 96,6% for SVM. Although their study involved 10 users and different gesture groups, some gestures are the same, such as “closed fist” and “index extended”.

To enhance the performance of the classifiers it is necessary to tune multiple variables. Starting on the data, where it needs to have more quality without have overlapping samples. The classifiers hyperparameter can be altered, in this work there weren’t change from the predefined ones in orange.

Chapter 5 - Conclusion and future perspectives

This work aimed to create an accessible, low cost and functional prosthetic hand using 3D printing and having control system with Arduino, to the help individuals that lost their hand and face difficulties in their everyday tasks.

The results of this work allowed to understand that the developed prosthetic was able to execute human gestures and to hold everyday objects. Despite being a fixed model due to it can easily be adapted or transform into a larger model and independent. The finger tests were a crucial phase, allowed to select the better motor and finger mechanism. The model C shows to provide the better results and due to that Model A and B were discard. If these two models were optimized, they could have shown better results. In Model A, replacing the torsion spring with a weaker one, and in Model B, changing the actuation system to a linear one, could have improved performance. However, all these improvements were left for future work. The assembled model needs to be optimized for an easy maintenance, every time it was necessary to fix something it was always needed to unassembled non-related parts.

The sensory component is assembled was tested and assembled in the prothesis but isn't active, by testing was possible to conclude that these systems work. The servo's force could be limited by the pressure applied in the A101 sensor and the alarm system was able to be activated when the temperature a value of 60ºC. The testing of these components in the assembled model was left for future work and it's crucial for the user to have these features in the final model because they will help to obtain information of grabbed objects. Regarding the A101 sensor, it is still necessary to calibrate the sensors inside the silicone, as it is possible that their sensitivity was affected. The work for a battery implementation was started when the current used by the servos was measured but it's necessary to quantify the consumption for all the components since and battery dimension in crucial to create portability and demolished the need for a power bench supply.

Regarding AI, this was the final part of the project, and it is the one that needs the more improvement. However, it was possible to create a dataset, segment it, extract features and train two classifiers. Despite not being able to implement in the prosthetic hand the human-machine interface a 91,2% accuracy from an NN and 87,4% from SVM was good result when comparing with the literature. These is always a tricky comparison because there a lot of variables that differ from the literature works. Normally the data is taken from large number of individuals, the feature and segmentation algorithms aren't the same. All of these factors will affect the final result. Nevertheless, it can be concluded that the classifiers need to be tested with optimized hyperparameters to determine which configuration achieves the best result. The collected data needs to have more quality, as some gesture acquisition sessions had poor

quality, and the overlap of EMG events compromised the segmentation process. More research efforts in this topic needs to be made and all these improvements were left for future work.

This work allowed to build a starting platform and to understand that are yet a lot of things to explore and future work to be done in this project.

Starting on the mechanical part, the forearm should be optimized to better accommodate all the electronics and to have a more anatomical correct size. The wrist needs a working articulation system. A better actuation system should be created something the utilizes a more direct actuation such as linear actuators. By combining it with a lever system, it will be possible to achieve more precise movement than what the string alone can provide. With this, the rubber bands system could be removed because the linear actuators could control both flexion and extension. In the area of actuation, further research could be conducted in the field of artificial muscles and soft robotics to take the system to the next step. The optimization of the fingertip design and the sensor encapsulation process is critical.

In the electronics is crucial to incorporate all the electronic components in a single PCB to keep everything in the same place and reduce the occupied space. The wiring needs to me thinner to reduce resistance imposed in the actuation system. The Arduino is a good platform and adapted to this work but with the introduction of AI a better and more powerful microcontroller need to be used like a Raspberry Pi. A wireless communication needs to be incorporated to allow for IoT capabilities in the prothesis. To achieve human-machine interface is necessary incorporate sEMG sensor in the prothesis.

In the field of AI, the dataset needs to be expanded in terms of sample size, improved in data quality and expanded to include a broader set of gestures. It is also important to more research to create a proper correlation between the muscle groups and the electrode placement to improve the data quality. Different hyperparameters in the ML models need to be tested and further model development should occur outside of the Orange platform. After this, the system must be able to transmit the real-time predictions to the actuators achieving a human-machine interface. Additionally, the AI model should be adaptive to the user, continuously collecting sEMG data while the prosthesis is in use and retraining itself to improve classification accuracy over time.

Bibliography References

[1] L. Trent *et al.*, “A narrative review: current upper limb prosthetic options and design,” Aug. 17, 2020, *Taylor and Francis Ltd*. doi: 10.1080/17483107.2019.1594403.

[2] L. Dunai, M. Novak, and C. G. Espert, “Human hand anatomy-based prosthetic hand,” *Sensors (Switzerland)*, vol. 21, no. 1, pp. 1–15, 2021, doi: 10.3390/s21010137.

[3] K. J. Zuo and J. L. Olson, “The evolution of functional hand replacement: From iron prostheses to hand transplantation,” *Plastic Surgery*, vol. 22, no. 1, p. 44, 2014, doi: 10.1177/229255031402200111.

[4] V. Putti, “Historical Prostheses,” *The Journal of Hand Surgery: British & European Volume*, vol. 30, no. 3, pp. 310–325, Jun. 2005, doi: 10.1016/J.JHSB.2005.01.001.

[5] F. Cordella *et al.*, “Literature review on needs of upper limb prosthesis users,” 2016, *Frontiers Media S.A.* doi: 10.3389/fnins.2016.00209.

[6] J. J. Stokosa, “Limb Prostheses Options Upper Limb Prostheses,” Mar. 2024. [Online]. Available: https://www.msdmanuals.com/home/special-subjects/limb-prosthetics/limb-prostheses-options

[7] B. Maat, G. Smit, D. Plettenburg, and P. Breedveld, “Passive prosthetic hands and tools: A literature review,” *Prosthet Orthot Int*, vol. 42, no. 1, pp. 66–74, Feb. 2018, doi: 10.1177/0309364617691622.

[8] N. Dechev, W. L. Cleghorn, and S. Naumann, “Multiple finger, passive adaptive grasp prosthetic hand,” *Mech Mach Theory*, vol. 36, no. 10, pp. 1157–1173, Oct. 2001, doi: 10.1016/S0094-114X(01)00035-0.

[9] “Otto Bock System Hand -passive- | Ottobock System Hands | Body Powered Systems | Upper Limb Prosthetics | Prosthetics | Ottobock CA Shop.” Accessed: Jul. 10, 2024. [Online]. Available: https://shop.ottobock.ca/en/Prosthetics/Upper-Limb-Prosthetics/Body-Powered-Systems/Ottobock-System-Hands/Otto-Bock-System-Hand--passive-/p/8K19

[10] “Adult Grip Prehensors - Fillauer TRS Prosthetics.” Accessed: Jul. 09, 2024. [Online]. Available: https://www.trsprosthetics.com/product/adult-grip-prehensors/

[11] “Better Choices for People with Partial Hand and Finger Loss.” Accessed: Jul. 09, 2024. [Online]. Available: https://www.armdynamics.com/upper-limb-library/better-choices-for-people-with-partial-hand-and-finger-loss

[12] “Introduction to Body-Powered Prostheses.” Accessed: Jul. 09, 2024. [Online]. Available: https://www.armdynamics.com/upper-limb-library/introduction-to-body-powered-prostheses

[13] V. H. Nagaraja, J. da Ponte Lopes, and J. H. M. Bergmann, “Reimagining Prosthetic Control: A Novel Body-Powered Prosthetic System for Simultaneous Control and Actuation,” Sep. 01, 2022, *MDPI*. doi: 10.3390/prosthesis4030032.

[14] W. Li, P. Shi, S. Li, and H. Yu, “Current status and clinical perspectives of extended reality for myoelectric prostheses: review,” 2023, *Frontiers Media SA*. doi: 10.3389/fbioe.2023.1334771.

[15] D. Huamanchahua *et al.*, “A robotic prosthesis as a functional upper-limb aid: An innovative review,” in *2021 IEEE International IOT, Electronics and Mechatronics Conference, IEMTRONICS 2021 - Proceedings*, Institute of Electrical and Electronics Engineers Inc., Apr. 2021. doi: 10.1109/IEMTRONICS52119.2021.9422648.

[16] “Myoelectric Prosthetic Hands.” Accessed: Jul. 10, 2024. [Online]. Available: https://www.ottobock.com/en-gb/myoelectric-prosthetics

[17] “Introduction to Myoelectric Prostheses.” Accessed: Jul. 10, 2024. [Online]. Available: https://www.armdynamics.com/upper-limb-library/introduction-to-myoelectric-prostheses

[18] “Ottobock | bebionic.” Accessed: Jul. 10, 2024. [Online]. Available: https://www.ottobock.com/en-gb/prosthetics/upper-limb-prosthetics/bebionic

[19] “Michelangelo hand | The Michelangelo hand helps you regain extensive freedom.” Accessed: Jul. 10, 2024. [Online]. Available: https://www.ottobock.com/en-us/product/8E500

[20] “i-Limb® Quantum Bionic Hand. Ossur.com.” Accessed: Jul. 10, 2024. [Online]. Available: https://www.ossur.com/en-us/prosthetics/arms/i-limb-quantum

[21] M. C. F. Castro, W. C. Pinheiro, and G. Rigolin, “A Hybrid 3D Printed Hand Prosthesis Prototype Based on sEMG and a Fully Embedded Computer Vision System,” *Front Neurorobot*, vol. 15, Jan. 2022, doi: 10.3389/fnbot.2021.751282.

[22] “What is a Hybrid Upper Limb Prosthesis?” Accessed: Jul. 10, 2024. [Online]. Available: https://www.armdynamics.com/upper-limb-library/what-is-a-hybrid-upper-limb-prosthesis

[23] “Introduction to Activity-Specific Prostheses.” Accessed: Jul. 10, 2024. [Online]. Available: https://www.armdynamics.com/upper-limb-library/an-introduction-to-activity-specific-prostheses

[24] H. Tabassum and K. Karnataka India Veena Saraf Assistant Professor, “A Low Cost Prosthetic Hand using Arduino and Servo Motors”, Accessed: Aug. 20, 2024. [Online]. Available: www.ijert.org

[25] G. Antonio Zappatore, G. Reina Politecnico di Bari, G. A. Zappatore, G. Reina, and A. Messina, “Analysis of a Highly Underactuated Robotic Hand,” *Article in International Journal of Mechanics and Control*, vol. XX, No. XX, p. 20, 2017, [Online]. Available: https://www.researchgate.net/publication/322082926

[26] T. Vanhuy *et al.*, “Simple Robotic Hand in Motion Using Arduino Controlled Servos Article in,” *International Journal of Science and Research (IJSR) ISSN*, vol. 6, 2017, doi: 10.21275/ART20171455.

[27] L. Dunai, M. Novak, and C. G. Espert, “Human Hand Anatomy-Based Prosthetic Hand,” *Sensors 2021, Vol. 21, Page 137*, vol. 21, no. 1, p. 137, Dec. 2020, doi: 10.3390/S21010137.

[28] S. Pitou, F. Wu, A. Shafti, B. Michael, R. Stopforth, and M. Howard, “Embroidered electrodes for control of affordable myoelectric prostheses,” *Proc IEEE Int Conf Robot Autom*, pp. 1812–1817, 2018, doi: 10.1109/ICRA.2018.8461066.

[29] D. Lanigan and Y. Tadesse, “Low Cost Robotic Hand that Senses Heat and Pressure,” 2017.

[30] L. Morales and J. Cepeda, “Feature extraction from sEMG of forearm muscles, performance analysis of neural networks and support vector machines for movement classification,” in *ICINCO 2017 - Proceedings of the 14th International Conference on Informatics in Control, Automation and Robotics*, SciTePress, 2017, pp. 254–261. doi: 10.5220/0006429402540261.

[31] R. K. Chen, Y. an Jin, J. Wensman, and A. Shih, “Additive manufacturing of custom orthoses and prostheses-A review,” *Addit Manuf*, vol. 12, pp. 77–89, 2016, doi: 10.1016/j.addma.2016.04.002.

[32] M. R. Aryal and S. Pun, “Additive manufacturing of prosthetic hands: a brief overview,” *International Journal on Interactive Design and Manufacturing*, vol. 16, no. 3, pp. 1099–1112, 2022, doi: 10.1007/s12008-022-00857-6.

[33] J. J. Cabibihan, M. K. Abubasha, and N. Thakor, “A Method for 3-D Printing Patient-Specific Prosthetic Arms with High Accuracy Shape and Size,” *IEEE Access*, vol. 6, pp. 25029–25039, Apr. 2018, doi: 10.1109/ACCESS.2018.2825224.

[34] K. V. Wong and A. Hernandez, “A Review of Additive Manufacturing,” *ISRN Mechanical Engineering*, vol. 2012, pp. 1–10, 2012, doi: 10.5402/2012/208760.

[35] D. W. Abbot, D. V. V. Kallon, C. Anghel, and P. Dube, “Finite element analysis of 3D printed model via compression tests,” *Procedia Manuf*, vol. 35, no. Smpm, pp. 164–173, 2019, doi: 10.1016/j.promfg.2019.06.001.

[36] T. D. Ngo, A. Kashani, G. Imbalzano, K. T. Q. Nguyen, and D. Hui, “Additive manufacturing (3D printing): A review of materials, methods, applications and challenges,” *Compos B Eng*, vol. 143, no. December 2017, pp. 172–196, 2018, doi: 10.1016/j.compositesb.2018.02.012.

[37] N. Divakaran, J. P. Das, A. K. P V, S. Mohanty, A. Ramadoss, and S. K. Nayak, “Comprehensive review on various additive manufacturing techniques and its implementation in electronic devices,” 2022. doi: 10.1016/j.jmsy.2022.01.002.

[38] “Arduino Nano — Arduino Official Store.” Accessed: Jun. 21, 2024. [Online]. Available: https://store.arduino.cc/products/arduino-nano

[39] “Arduino Uno Rev3 — Arduino Official Store.” Accessed: Jun. 21, 2024. [Online]. Available: https://store.arduino.cc/products/arduino-uno-rev3

[40] “Arduino Mega 2560 Rev3 — Arduino Official Store.” Accessed: Jun. 21, 2024. [Online]. Available: https://store.arduino.cc/products/arduino-mega-2560-rev3

[41] A. Shakirovich Ismailov Zafar Botirovich Jo, “Study of arduino microcontroller board”, Accessed: Aug. 21, 2024. [Online]. Available: www.openscience.uz

[42] Y. A. Badamasi, “The working principle of an Arduino,” *Proceedings of the 11th International Conference on Electronics, Computer and Computation, ICECCO 2014*, Dec. 2014, doi: 10.1109/ICECCO.2014.6997578.

[43] “Arduino Uno Rev3 — Arduino Official Store.” Accessed: Nov. 09, 2023. [Online]. Available: https://store.arduino.cc/products/arduino-uno-rev3

[44] “What is Arduino? | Arduino.” Accessed: Nov. 06, 2023. [Online]. Available: https://www.arduino.cc/en/Guide/Introduction

[45] “Inter-Integrated Circuit (I2C) Protocol | Arduino Documentation.” Accessed: Jul. 15, 2024. [Online]. Available: https://docs.arduino.cc/learn/communication/wire/

[46] J. Seaton and C. Leach, “Local property measurement in PTC thermistors,” *Acta Mater*, vol. 51, no. 20, pp. 6027–6034, Dec. 2003, doi: 10.1016/S1359-6454(03)00387-2.

[47] G. Liu, L. Guo, C. Liu, and Q. Wu, “Evaluation of different calibration equations for NTC thermistor applied to high-precision temperature measurement,” *Measurement*, vol. 120, pp. 21–27, May 2018, doi: 10.1016/J.MEASUREMENT.2018.02.007.

[48] A. Ashraf, A. Halim, M. N. Hassan, A. Zakaria, and L. M. Kamarudin, “Internet of things technology for greenhouse monitoring and management system based on wireless sensor network.” [Online]. Available: https://www.researchgate.net/publication/320857964

[49] “LM35 Precision Centigrade Temperature Sensors - Datasheet,” 1999, Accessed: Aug. 21, 2024. [Online]. Available: www.ti.com

[50] “NTC 100kR 3.5mW Ø3mm.” Accessed: Aug. 21, 2024. [Online]. Available: https://mauser.pt/catalog/product_info.php?products_id=095-0101

[51] “B59870C0080A070 - Epcos - PTC Thermistor, 25 ohm, Through Hole.” Accessed: Aug. 21, 2024. [Online]. Available: https://pt.farnell.com/epcos/b59870c0080a070/ptc-thermistor-25r-tht/dp/2769016

[52] “LM35DZ/LFT4 Texas Instruments | Mouser Portugal.” Accessed: Aug. 21, 2024. [Online]. Available: https://pt.mouser.com/ProductDetail/Texas-Instruments/LM35DZ-LFT4?qs=QbsRYf82W3FEZkSvxC%252BtOg%3D%3D

[53] “Piezoresistive Sensor - an overview | ScienceDirect Topics.” Accessed: Aug. 21, 2024. [Online]. Available: https://www.sciencedirect.com/topics/engineering/piezoresistive-sensor

[54] “Force Sensors | Tekscan.” Accessed: Aug. 21, 2024. [Online]. Available: https://www.tekscan.com/force-sensors

[55] “FlexiForce Load/Force Sensors and Systems | Tekscan.” Accessed: Aug. 21, 2024. [Online]. Available: https://www.tekscan.com/flexiforce-loadforce-sensors-and-systems

[56] “Mini Force Sensing Resistor | FlexiForce A101 Sensor | Tekscan.” Accessed: Aug. 21, 2024. [Online]. Available: https://www.tekscan.com/products-solutions/force-sensors/flexiforce-a101-sensor

[57] G. Di Pasquo, “SG90 Servo Characterization”.

[58] “SG90 Datasheet(PDF) - List of Unclassifed Manufacturers.” Accessed: Aug. 22, 2024. [Online]. Available: https://www.alldatasheet.es/datasheet-pdf/pdf/1572383/ETC/SG90.html

[59] L. Dunai, M. Novak, and C. G. Espert, “Human hand anatomy-based prosthetic hand,” *Sensors (Switzerland)*, vol. 21, no. 1, pp. 1–15, Jan. 2021, doi: 10.3390/s21010137.

[60] “MG995 Datasheet, PDF - Alldatasheet.” Accessed: Aug. 22, 2024. [Online]. Available: https://www.alldatasheet.com/view.jsp?Searchword=Mg995%20datasheet&gad_source=1&gclid=Cj0KCQjww5u2BhDeARIsALBuLnM47I4Ff6aaQSlwnbFXjjGRL53vGCWvkSWYTtG-NzkSG0BoCrzGa7waAmGUEALw_wcB

[61] Z. Koudelkova *et al.*, “Verification of Finger Positioning Accuracy of an Affordable Transradial Prosthesis,” *Designs (Basel)*, vol. 7, no. 1, Feb. 2023, doi: 10.3390/designs7010014.

[62] “Motor micro servo 4.8V..6V DC SG90 - 180º.” Accessed: Aug. 22, 2024. [Online]. Available: https://mauser.pt/catalog/product_info.php?products_id=096-6477

[63] “MG995 Micro Digital Servo Motor for RC Robot helicopter aircraft.” Accessed: Aug. 22, 2024. [Online]. Available: https://www.az-delivery.de/en/products/az-delivery-servo-mg995?_pos=1&_sid=9845b6c3a&_ss=r

[64] F. Gaetani, G. A. Zappatore, P. Visconti, and P. Primiceri, “Design of an Arduino-based platform interfaced by Bluetooth low energy with Myo armband for controlling an under-actuated transradial prosthesis,” in *ICICDT 2018 - International Conference on IC Design and Technology, Proceedings*, Institute of Electrical and Electronics Engineers Inc., Jun. 2018, pp. 185–188. doi: 10.1109/ICICDT.2018.8399787.

[65] P. Visconti, F. Gaetani, G. A. Zappatore, and P. Primiceri, “Technical features and functionalities of Myo armband: An overview on related literature and advanced applications of myoelectric armbands mainly focused on arm prostheses,” *International Journal on Smart Sensing and Intelligent Systems*, vol. 11, no. 1, pp. 1–25, 2018, doi: 10.21307/ijssis-2018-005.

[66] F. Silva De Moura, D. C. Soriano, S. Masson, F. S. Fortuna, F. S. Moura, and D. C. Soriano, “INTEGRATING MYO ARMBAND FOR THE CONTROL OF MYOELECTRIC UPPER LIMB PROSTHESIS,” 2016. [Online]. Available: https://www.researchgate.net/publication/309415054

[67] M. Cognolato *et al.*, “Hand Gesture Classification in Transradial Amputees Using the Myo Armband Classifier,” in *Proceedings of the IEEE RAS and EMBS International Conference on Biomedical Robotics and Biomechatronics*, IEEE Computer Society, Oct. 2018, pp. 156–161. doi: 10.1109/BIOROB.2018.8488106.

[68] J. S. Hussain, A. Al-Khazzar, and M. N. Raheema, “Recognition of new gestures using myo armband for myoelectric prosthetic applications,” Dec. 01, 2020, *Institute of Advanced Engineering and Science*. doi: 10.11591/ijece.v10i6.pp5694-5702.

[69] C. Janiesch, P. Zschech, and K. Heinrich, “Machine learning and deep learning”, doi: 10.1007/s12525-021-00475-2/Published.

[70] K. Sharifani and M. Amini, “Machine Learning and Deep Learning: A Review of Methods and Applications.” [Online]. Available: https://ssrn.com/abstract=4458723

[71] I. H. Sarker, “Machine Learning: Algorithms, Real-World Applications and Research Directions,” May 01, 2021, *Springer*. doi: 10.1007/s42979-021-00592-x.

[72] P. Amin, A. M. Khan, A. R. Bhat, and G. Rao, “Feature Extraction and Classification of Gestures from Myo-Electric Data Using a Neural Network Classifier,” in *Advances in Intelligent Systems and Computing*, Springer Science and Business Media Deutschland GmbH, 2021, pp. 65–80. doi: 10.1007/978-981-15-5788-0_7.

[73] R. Y. Choi, A. S. Coyner, J. Kalpathy-Cramer, M. F. Chiang, and J. Peter Campbell, “Introduction to machine learning, neural networks, and deep learning,” *Transl Vis Sci Technol*, vol. 9, no. 2, 2020, doi: 10.1167/tvst.9.2.14.

[74] R. Dastres and M. Soori, “Artificial Neural Network Systems,” 2021. [Online]. Available: www.ceserp.com/cp-jour

[75] A. Roy and S. Chakraborty, “Support vector machine in structural reliability analysis: A review,” *Reliab Eng Syst Saf*, vol. 233, p. 109126, May 2023, doi: 10.1016/J.RESS.2023.109126.

[76] P. Chhajer, M. Shah, and A. Kshirsagar, “The applications of artificial neural networks, support vector machines, and long–short term memory for stock market prediction,”

Decision Analytics Journal, vol. 2, p. 100015, Mar. 2022, doi: 10.1016/J.DAJOUR.2021.100015.

[77] N. Huda Ovirianti, M. Zarlis, and H. Mawengkang, “Support Vector Machine Using A Classification Algorithm,” *Jurnal dan Penelitian Teknik Informatika*, vol. 7, no. 3, 2022, doi: 10.33395/sinkron.v7i3.

[78] “Original Prusa MINI+ Semi-assembled 3D Printer | Original Prusa 3D printers directly from Josef Prusa.” Accessed: Aug. 15, 2024. [Online]. Available: https://www.prusa3d.com/product/original-prusa-mini-semi-assembled-3d-printer-4/

[79] “Anycubic Kobra 2 Pro: Maximum Print Speed up to 500mm/s Standard Size 3D Printer.” Accessed: Aug. 15, 2024. [Online]. Available: https://store.anycubic.com/products/kobra-2-pro

[80] “GitHub - muhammetduzenli/myo-emg-data-recorder: EMG and IMU data recorder GUI for MYO Armband.” Accessed: Aug. 14, 2024. [Online]. Available: https://github.com/muhammetduzenli/myo-emg-data-recorder

[81] “Myo Connect 0.9 beta - Myo Connect.exe.” Accessed: Aug. 14, 2024. [Online]. Available: https://myo-connect.software.informer.com/0.9b/